NUCLEAR ENGINEERING
READING ROOM - M.I.T.

MITNE-246

BWR DEPLETION METHODS USING QUANDRY AND THE RESPONSE MATRIX TECHNIQUE OF ASSEMBLY HOMOGENIZATION

by

Hussein Khalil

May 20, 1981

1. Introduction

The success of nodal methods in solving accurately and efficiently the few-group diffusion equations combined with recent advances in the calculation of homogenized nodal cross sections provide motivation for extending these methods to the performance of depletion calculations. Furthermore, since in present state-of-the-art depletion packages, isotopes are generally depleted from regions of a reactor by the neutron flux averaged over a large "depletion block", the use of nodal schemes becomes even more attractive. Although FLARE-type nodal programs have been used to perform full-core spatial calculations in depletion models, these codes use a crude neutronics analysis, relying heavily on empirically adjusted "transport kernels" and boundary albedoes to match results of higher-order calculations.[1] Although when tuned in this manner, these codes can give a satisfactory description of reactor performance over life, confidence in these results is somewhat limited, and application of the various empirical adjustments outside ranges where they have been verified is not possible.

Presently, an EPRI-sponsored study is underway at MIT to extend the use of the nodal code QUANDRY[2] to performance of the spatial calculation in a depletion model. QUANDRY has a strong theoretical foundation and relies on only one basic approximation in which the transverse leakage from a node is assumed to be quadratic in shape. The code has been tested using a large variety of LWR multi-dimensional static and transient benchmark problems, and its accuracy and speed have been clearly demonstrated.

As with all nodal models QUANDRY requires cross sections that are constant within the individual nodes, and thus errors in highly heterogeneous problems (particularly BWR's) can be encountered because of the inadequacy of conventional methods of cross section homogenization[3] (e.g. simple flux-weighting of heterogeneous cross sections by the flux computed in an isolated-assembly calculation with $\underline{J}\cdot\underline{n} = 0$ boundary conditions). However, Koebke[4] has shown that it is possible to define equivalent homogenized nodal parameters that will reproduce in a nodal calculation all reaction rates and the global reactor eigenvalue of a reference fine-mesh solution. Although the calculation of these exact parameters would require actually performing the heterogeneous full-core solution (and would thus be self-defeating), methods have been developed to obtain good approximations of the formally-exact values. In particular, Smith has generalized and simplified somewhat Koebke's equivalence theory method and incorporated the revised model into QUANDRY[3]. This generalized method is applied by first performing isolated-assembly calculations for each node in the system to determine flux-weighted cross sections and discontinuity factors (which can be viewed as additional homogenized parameters in a node). These assembly discontinuity factors (ADF) and assembly-homogenized cross sections (AHCS) are then used to perform a global homogenized (QUANDRY) calculation to obtain a first estimate of the net surface currents on the boundaries of the various assemblies. These currents can then be imposed on the assemblies in heterogeneous, fixed-source calculations to obtain improved estimates of the exact HCS and DF which are in turn used in another global calculation, and the procedure can in principle be repeated until convergence of the global solution. The converged (or nearly converged) global results have been shown to match very closely results obtained by solving the reference global heterogeneous problem.

Cheng[5] has developed a system of computer programs in which the response matrix (RM) method is used to update the homogenized cross sections (HCS) and discontinuity factors (DF). The "response" of any heterogeneous assembly (i.e. detailed group fluxes and interaction rates) to unit net surface currents in each group and over different segments of the node surface can be precalculated by performing a series of fine-mesh fixed-source calculations for the node in question. In present applications, the shape of the net current over each segment is assumed to be flat. The response matrices can be used in conjunction with actual net surface currents (from a nodal full-core calculation) in local calculations for the various assemblies to update the HCS and DF. The method relies on the fact that the "responses" to currents of arbitrary amplitude applied to nodal surfaces can be found by superposition and thus accounts for the effects of boundary currents on the node homogenized parameters without the need to repeat relatively expensive fixed-source diffusion calculations for identical assemblies in different core locations.

The local calculations for the various assemblies are performed using the code RESPONSE[5], in which group net currents from the global problem can be distributed over the various segments of the node surface. These RM calculations can be performed for an individual node or for a five-node cluster in which effects due to nearest neighbors on the current shape at the boundary of the center-node are modeled (and thus the two-segment approach becomes useful).

Benchmark calculations using the RM's to update the HCS and DF have shown that even for extremely heterogeneous cases, the use of one-node local calculations and one global/local iteration reduced the maximum error in nodal power to ∿ 2%, a considerable improvement over ADF results (∿ 5% errors) and a drastic improvement over conventional flux-weighting schemes (∿ 15% errors).

In this report, a method is described for extension of QUANDRY and the RM technique of assembly homogenization to BWR depletion studies. Several problems are considered, including the variation of RM elements with important variables in the depletion calculations (such as nodal exposure E and coolant void fraction v) and possible interpolation and data manipulation techniques. Finally, some anticipated problems with the overall method and potential solutions are presented. However, before commencing with these topics, a description of conventional depletion methods is given.

2. Review of Depletion Methods

The great diversity in methods used to perform depletion calculations (and the fact that they are frequently company confidential) makes it difficult to give a detailed account of existing depletion methods. However, it seems possible to group the various methods into two distinct approaches depending on whether isolated-assembly depletion calculations are performed prior to the actual full-core depletion calculation. In the first of these (Method 1), assembly depletions are not performed, and zero-dimensional depletion runs are used to create tables of microscopic, few-group cross sections as a function of exposure, as well as other important properties (temperature, moderator density, etc.) for each initially different type of fuel cell (or some larger portion of an assembly) present in the core. These cross section tables, which account in an approximate manner for effects of spectral changes on the few-group cross sections during lifetime, are then used in tandem with a spatial-diffusion/depletion computation. Either "point" or "block" depletions may be performed depending on whether number densities and macroscopic cross sections are updated for individual fuel cells or for larger regions (using the neutron flux averaged over that region).

With the second depletion approach (Method 2), each cell in an assembly is modeled explicitly in a two-dimensional assembly depletion calculation in which neutron leakage at the node boundaries is assumed zero over life. This assumption of no leakage, while never completely justified, is generally accepted for BWR's and is frequently made for PWR's as well. Each assembly is thus effectively decoupled from its environment, and assembly parameters such as k_∞ and heterogeneous, macroscopic, few-group cross sections may be tabulated -- again as functions of exposure and other assembly properties. Tables of this type greatly ease the "bookkeeping" tasks in fine-mesh depletion calculations, but their accuracy obviously depends on the mathematical model employed in the assembly depletion runs. Method 2 is also very useful when nodal methods are used to perform the global depletion computation, since the assembly depletion results may be averaged to yield nodal parameters as a function of burnup.

Clearly, the two methods overlap significantly (for example, Method 1 may be employed on the assembly level with a point depletion option to perform the assembly depletions required for Method 2), and thus many of the calculational procedures are applicable to both. Both of these methods and some of the computer codes used in their implementation are discussed below. However, for more detailed discussions of the various codes, the reader is advised to consult the program manuals and the references cited therein. Also, no attempt is made to review the enormous topic of basic cross section data reduction techniques. An excellent (but slightly dated) discussion of these methods is given in the review article by Adensam et al.[6]

2.1 Method 1

The first step in this approach is the use of multi-group cross-sectional data to perform spectrum calculations for the various depleting regions over life. The neutron slowing down spectrum is typically computed using a P-1 or B-1 approximation to the Fourier transformed Boltzmann equation[7], while the thermal spectrum is most commonly evaluated using the Wigner-Wilkins[8] model. Thus, tables of few-group, region-averaged, microscopic cross sections can be generated as a function of exposure for each region. The depletion calculations are performed for a zero-dimensional system, with leakage approximated by DB_r^2 (B_r^2 = geometric buckling). LEOPARD[9] is perhaps the most well-known of the codes that perform this task. In LEOPARD, cell heterogeneity is simulated by use of fast advantage factors, thermal disadvantage factors, and resonance self-shielding factors. A more accurate representation of this heterogeneity is possible if collision probability or other transport theory methods are used (as is done in the EPRI-CELL code[10], for example). Fission product buildup is usually treated by lumping all fission products (other than Xe and Sm) into a single material and adjusting their effective absorption cross section to match more sophisticated burnup-lifetime calculations. Although less famous than LEOPARD, other zero-dimensional burnup codes such as LASER[11] and CINDER[12] also exist and perform many of the same calculations with varying degrees of sophistication and accuracy. Strong absorbers (i.e. control rods, burnable poison rods) require auxiliary calculations generally based on blackness theory[13] and are performed by RODWORTH[14], MICBURN[15], and other codes.

Spatial calculations at the beginning of each depletion time step are performed by solving the few-group diffusion equations using standard finite-difference codes such as PDQ-7[16] or CITATION[17]. The computed flux shape (to be used to deplete the isotopes) must correspond to the full-power operating conditions of the reactor, with control rods in their proper positions (or the concentration of burnable poison adjusted for criticality) and the coolant density and temperature profiles consistent with the power distribution. Clearly, an iterative procedure is required, and in view of the enormous expense of performing full-core, finite-difference diffusion calculations, auxiliary methods and numerous tricks are used to reduce the frequency and expense of these calculations[7]. Generally, pin-by-pin heterogeneity is not modeled explicitly, and macroscopic cross sections are assigned to regions of the reactor that are similar at the beginning of life (depletion blocks). The computed, power-normalized group fluxes are then averaged over each depletion block, and the resulting average fluxes are used to deplete the isotopes in that region over a chosen depletion time step.

The isotope depletion calculational procedure may be described by considering specifically the program HARMONY[16] adjunct to PDQ-7. In this code, the fluxes from the spatial calculation are used to solve a set of differential equations that describe the time-variation of the nuclide concentrations during the depletion interval. At the end of this interval, the computed number densities can be used together with the pre-tabulated microscopic cross sections to recompute the few-group macroscopic cross sections for the ensuing spatial calculation. In solving these equations, allowance is made for step-wise time-dependence of microscopic cross sections within a depletion step by interpolation of the pre-generated cross section tables. Constant power operation is simulated by thermal flux renormalization, a procedure that also reduces the required frequency of spatial calculations.

2.2 Method 2

Although zero-dimensional codes can model whole-assembly depletions in an approximate and empirically adjusted manner[9], increases in computer capabilities have made the use of more accurate methods based on transport theory and collision probability techniques more attractive. Methods have been developed to deal simultaneously with a number of adjacent cells in an assembly and with entire assemblies. With an assembly, multigroup spectra are obtained (at B.O.L.) by solution of the space-energy transport equation (e.g. using collision probability techniques) for the different pin cells. These spectra are used for cross sectional energy condensation and spatial homogenization within the individual cells. Special calculations are required for treatment of resonance cross sections and strongly absorbing regions. Few-group cross sections smeared over the different cells are then used in 2-D spatial calculations, in which the integral transport equation is solved with $\underline{J}\cdot\underline{n} = 0$ conditions imposed at the assembly boundaries. With the resultant scalar flux distribution, assembly homogenized cross sections may be obtained and the depletion equations can be solved for the different fuel-containing cells. The new number densities are then used to repeat the entire procedure at a new value of assembly exposure.

Methods of this type have been incorporated into codes such as Combustion Engineering's DIT program[18] and EPRI's CPM[19] and CASMO[20]. The output from these codes typically consists of nodal k_∞, heterogeneous fluxes, and macroscopic cross sections for each fuel cell (as well as non-fueled regions) in an assembly as a function of exposure and other assembly properties. These same results can also be obtained (although less accurately) by performing assembly depletion calculations using a diffusion/depletion model on the assembly level. Results of the assembly calculations can then be used in global finite-difference diffusion calculations or may be collapsed to yield assembly-averaged data for use in nodal codes.

Because of the enormous expense of full-core, finite-difference calculations, the use of nodal codes of the FLARE type to perform three dimensional spatial calculations in depletion models has become quite standard. These codes are capable of predicting reactivity, power and void distributions, and critical control rod positions throughout life by using very coarse mesh spacings. The great economy of these codes also permits calculation of assembly flow rates and optimized fuel loading patterns based on desired power shapes and overall fuel management objectives.

The nodal codes presently used adopt an extremely simple approach to core neutronics. Typically, a one-group neutron balance is performed for each node j and may be written (in a somewhat simplified form) as[21]

$$A_j = \sum_j W_{mj} S_m = \sum_{m \neq j} W_{mj} S_m + W_{jj} S_j \tag{1}$$

$$S_j = \frac{1}{\lambda} k_{\infty,j} A_j \tag{2}$$

where

S_j ≡ rate of neutron production by fission in node j

A_j ≡ rate of neutron loss by absorption in node j

W_{mj} ≡ probability that a neutron born in node m is absorbed in node j ($\sum_j W_{mj} = 1$)

and λ ≡ global reactor eigenvalue.

To reduce further the computational effort, it is customary (but not necessary) to assume only nearest-neighbor coupling in Eq. (1). Also, the "transport kernels" W_{mj} are usually synthesized in simple ways using the neutron migration area M^2 ($\equiv \frac{D_1}{\Sigma_{a1}+\Sigma_{21}} + \frac{D_2}{\Sigma_{a2}}$) and the node size and then adjusted by a blend of theoretical analysis and empiricism. For depletion calculations, the nodal parameters (e.g. k_∞, M^2) are computed as functions of exposure and other node properties using polynomial coefficients predetermined by fitting results of the previously-performed assembly depletions.

Because of the simple neutronic model, the FLARE-tupe codes often given unsatisfactory results. Errors in nodal powers of 2% and upward are not uncommon[22]. It should be noted, however, that improved but proprietary versions of FLARE are known to exist. Also, the basic FLARE model has been expanded into other nodal codes (e.g. TRILUX[23], PRESTO[24], SIMULATE[25]). TRILUX, for example, is capable of treating larger cores, calculating additional quantities of interest (e.g. critical heat flux ratios), and utilizing more complicated fits of k_∞ as a function of exposure and other nodal properties.

3. BWR Depletions Using QUANDRY

The basic techniques presently used to perform BWR depletions using nodal methods are directly applicable to a depletion model in which QUANDRY performs the spatial, full-core solution. The primary differences are the use of a more rigorous neutronic model and a more accurate assembly homogenization technique. However, implementation of these procedures requires no change in the depletion model.

3.1 General Description of the Method

3.1.1 Assembly Depletion Calculations. As in conventional nodal depletion models, a two-dimensional assembly depletion calculation with $\underline{J}\cdot\underline{n} = 0$ boundary conditions over the entire lifetime of the assembly will suffice for each initially different assembly loaded in the core. Although this neglects the possibly significant flux tilts that an assembly experiences during its in-core residence, it is generally agreed that for the purposes of determining heterogeneous, macroscopic cross sections throughout life, this approximation is justified. These cross sections can then be used in fixed-source calculations to obtain nodal response matrices as a function of exposure (see Section 3.1.2). In addition, it is possible to edit out of these calculations the AHCS and ADF as functions of exposure E using

$$\text{AHCS} \equiv \bar{\Sigma}^k_{\alpha g}(E) = \frac{\int_{V_k} \Sigma_{\alpha g}(\underline{r},E)\ \phi_g(\underline{r},E)dV}{\bar{\phi}^k_g(E)\ V_k} \tag{3}$$

$$\text{ADF} \equiv f^{k}_{g\ell}(E) \equiv \frac{\int_{S_\ell} \phi_g(\underline{r},E)\, dS}{\bar{\phi}^{k}_{g}(E)\, V_k} \tag{4}$$

where $$\bar{\phi}^{k}_{g}(E) = \frac{1}{V_k}\int_{V_k} \phi_g(\underline{r},E)\, dV \tag{5}$$

and where α denotes the type of interaction, k is an assembly index, ℓ refers to the ℓ^{th} surface of assembly k, and the remaining notation is standard.

For BWR's, these assembly depletions must be performed for several assumed values of coolant void fraction u and for both the rodded and unrodded configurations of the (two-dimensional) assembly "slice". By keeping u constant during the depletion, the void history of the node defined by

$$v = \frac{1}{E}\int_{0}^{E} u(E')\, dE' \tag{6}$$

is also fixed (and simply equals u). To account for instantaneous voids which may differ from v, "branch calculations" are performed at various exposure intervals. In these calculations, number densities obtained from the main depletion sequence are retained for all materials except the coolant. These densities and the adjusted water density are used together with appropriately modified few-group microscopic cross sections to recompute spatial flux distributions at the various exposures. Similar branch calcullations in which the fuel temperature is varied, or the control blade is inserted (or withdrawn) are useful for determining effects of these variables on the assembly depletion results.

3.1.2 Response Matrix Considerations. Once the heterogeneous macroscopic cross sections are known for an assembly throughout life, the RM's for that node may be generated as a function of exposure and other nodal properties (including the global eigenvalue). The required matrices for node k are denoted by [R], $[\hat{R}]$, and $[\tilde{R}]$ and are defined by

$$[\overline{\phi}^S]_k = [R]_k[J] \tag{7}$$

$$[F]_k = [\hat{R}]_k[J] \tag{8}$$

$$[M]_k = [\tilde{R}]_k[J] \tag{9}$$

In these equations, [J] is a column vector of group net surface currents in the outward normal direction to various segments on the four faces of a (two-dimensional) node. Thus, for a G-group, N-segment per face model, [J] may be expressed as

$$[J] \equiv \text{Col}\ \{J_{(n-1)G+g}\} \qquad g = 1, \ldots, G \qquad n = 1, \ldots, 4N \tag{10}$$

The quantity $[\overline{\phi}^S]_k$ represents a column vector of nodal group fluxes averaged over various segments of the node surface, i.e.

$$[\bar{\phi}^S]_k \equiv \text{Col}\ \{\bar{\phi}^S_{(n-1)G+g}\} = \text{Col}\ \{\frac{1}{S_n}\int_{S_n}\phi_g(\underline{r})\ dS\}$$

$$g = 1, \ldots, G$$

$$n = 1, \ldots, 4n \qquad (11)$$

where S_n is the area of the n^{th} portion of the nodal surface. The matrix $[F]_k$ is defined as

$$[F]_k \equiv \text{Col}\ \{\int_{V_k}\Sigma_{\alpha g}\ \phi_g\ dV\ \}$$

$$\alpha = 1, \ldots, 6$$

$$g = 1, \ldots, G \qquad (12)$$

where the correspondence between α and $\Sigma_{\alpha g}$ is given by

$\alpha =$	1	2	3	4	5	6
$\Sigma_{\alpha g} =$	$1/D_g$	Σ_{tg}	$\Sigma_{gg'}$	$\nu\Sigma_{fg}$	Σ_{fg}	1

and where V_k is the volume of node k. Finally, $[M]_k$ is defined by the I-element column vector

$$[M]_k \equiv \text{Col} \quad \sum_{g=1}^{G}\int_{V_i \subset V_k}\Sigma_{fg}^{(i)}\phi_g\ dV$$

$$i = 1, \ldots, I \qquad (13)$$

where i denotes a fueled region within node k (and V_i its volume), and I is the total number of fuel cells contained within the node.

With this assignment of matrix elements, it is apparent that knowledge of the square matrix [R] and the non-square matrices $[\hat{R}]$ and $[\tilde{R}]$ together with net surface currents (from a global QUANDRY run, for example) gives information about the average of the heterogeneous surface flux (used for DF calculations), the node-integrated reaction rates (used for HCS calculation), and the local fission rates within an assembly (used for prediction of nuclear hot spot factors).

The fixed-source calculations needed to generate the response matrices can in principle be performed using any one of a number of mathematical models (e.g. Monte Carlo, multigroup transport theory, etc.). However, for consistency, the same model that is used to define the reference solution (i.e. the solution to be matched by the nodal (homogenized calculation) must also be used to generate the response matrices.[5]

3.1.3 Depletion Procedure. After the RM's have been generated for all required nodal conditions, actual depletion calculations may be performed by the following procedure:

i) Consider an initial core configuration with known nodal exposures.

ii) Obtain the ADF and AHCS for all nodes at reference values of nodal properties (including control blade presence and control history) by interpolation of pretabulated ADF and AHCS as functions of exposure.

iii) Perform a three-dimensional global QUANDRY calculation (with unity DF in the Z-direction) to obtain consistent void v and temperature T distributions, as well as the global eigenvalue λ_g.

iv) Interpolate the available, precomputed RM's for each node to the proper T, v, and λ_g at the known nodal exposures. Use these matrices together with the net surface currents computed by QUANDRY in local, response matrix calculations to obtain improved estimates of the HCS and DF.[5]

v) Rerun the global (QUANDRY) calculation using the revised HCS and DF (again with thermal-hydraulic feedback) to obtain updated currents, thermal hydraulic variables, and λ_g.

vi) Repeat steps iv and v until satisfactory convergence of the global solution is achieved.*

vii) If λ_g differs from unity, return to step ii and repeat the procedure with control blade positions adjusted so that the critical condition is approached.

viii) Use the converged, critical net current distributions together with the matrices $[R]_k$ (see Eqs. (9) and (13)) to obtain the local fission rates needed to determine the location and magnitude of the peak local power.

---

*Since a criticality search must still be performed, it may be undesirable at this stage to converge the global solution fully.

ix) For a given depletion (calendar) interval, determine the energy removed from each assembly using the converged, critical power distribution found in step vi.

x) Return to step ii with the exposure distribution (found in step ix) and the nodal properties (found in step vi) to obtain the ADF and AHCS needed for the first global solution at the beginning of the second depletion time step.

xi) Repeat the procedure of steps ii to x until the end of the operating cycle.

xii) Return to step i for the beginning of the next operating cycle.

This procedure provides nearly all quantities of interest in a reactor analysis model. In particular fuel loading patterns, control strategies, and thermal hydraulic parameters can be evaluated, and their consistency with overall fuel management objectives can be assessed.

3.2 Specific Considerations

The methods described in Section 3.1 are quite general, and thus it is desirable at this point to consider a few points in more detail.

3.2.1 Assembly Depletions. The initial assembly depletion calculations may be performed by use of either an assembly depletion code (e.g. CASMO) or a general diffusion/depletion model applied to individual assemblies with $\underline{J} \cdot \underline{n} = 0$ boundary conditions (e.g. LEOPARD - PDQ/HARMONY). These assembly depletions are typically performed for three assumed values of coolant void fraction (v=0, 0.4, and 0.7) and for both the rodded and unrodded configuration of each assembly. Cross sectional data (both heterogeneous and flux-weighted), the ADF, and the nodal k_∞ may be obtained from these calculations at discrete values of exposure (e.g. E=0, 5, 10, 20, and 30 MWD/kg) and can be obtained for intermediate exposures using low-order polynomial fits. Branch calculations, which account for fuel temperature, instantaneous void, and control history effects, are usually performed at these same discrete nodal exposure values.[26]

3.2.2 Response Matrix Generation. Response matrices can be generated by solution of a number of fixed-source problems for each assembly with different "external" source distributions to simulate the various group net currents imposed on each segment of the assembly's surfaces. Since the matrices are computed for the purpose of determining homogenized parameters that would reproduce in a nodal calculation the reaction rates and the global eigenvalue of some chosen reference solution (e.g. a finite-difference, few-group, diffusion theory result), the same energy and spatial approximations that characterize this reference solution must be made in generation of the response matrices. Thus, a fine-mesh, few-group, diffusion theory approximation is used in performing the fixed-source calculations which are needed to compute the response matrices. The code CITATION is particularly well suited for this task because it has the capability of solving the diffusion equation with an "external" source term in a multiplying medium and because it allows the group fluxes to be negative (as is required for neutron balance in a subcritical assembly with an imposed net current in the outward direction). Sample input data for CITATION are given in Appendix 1, together with details of Cheng's procedure for response matrix generation given the heterogeneous cross sections corresponding to fixed values of assembly conditions (including λ_g). For more theoretical details, the reader should consult Cheng's doctoral thesis.[5]

3.2.2 Global/Local Iteration. Even though each iteration between the global (QUANDRY) and local (RESPONSE) calculations is quite fast[5], it is clearly desirable to perform a minimum number of these iterations. Cheng has shown that for B.O.L. conditions and no thermal-hydraulic feedback, nodal powers and global eigenvalue are accurately predicted if only one iteration is performed and if single node local calculations are used. Whether this simple procedure will prove satisfactory over life (and for cases where thermal hydraulic feedback effects are significant and where local power information is desired) is a question that remains to be answered.

Some details of the calculational steps used in actual implementation of the global/local iteration are given in Appendix 2.

3.2.3 Summary. A flow diagram illustrating the overall procedure for the proposed depletion model is given in Fig. 1.[*]

---

[*] This diagram is somewhat simplified because the calculational steps needed to perform a criticality search or an adjustment of the fuel loading pattern are not shown explicitly.

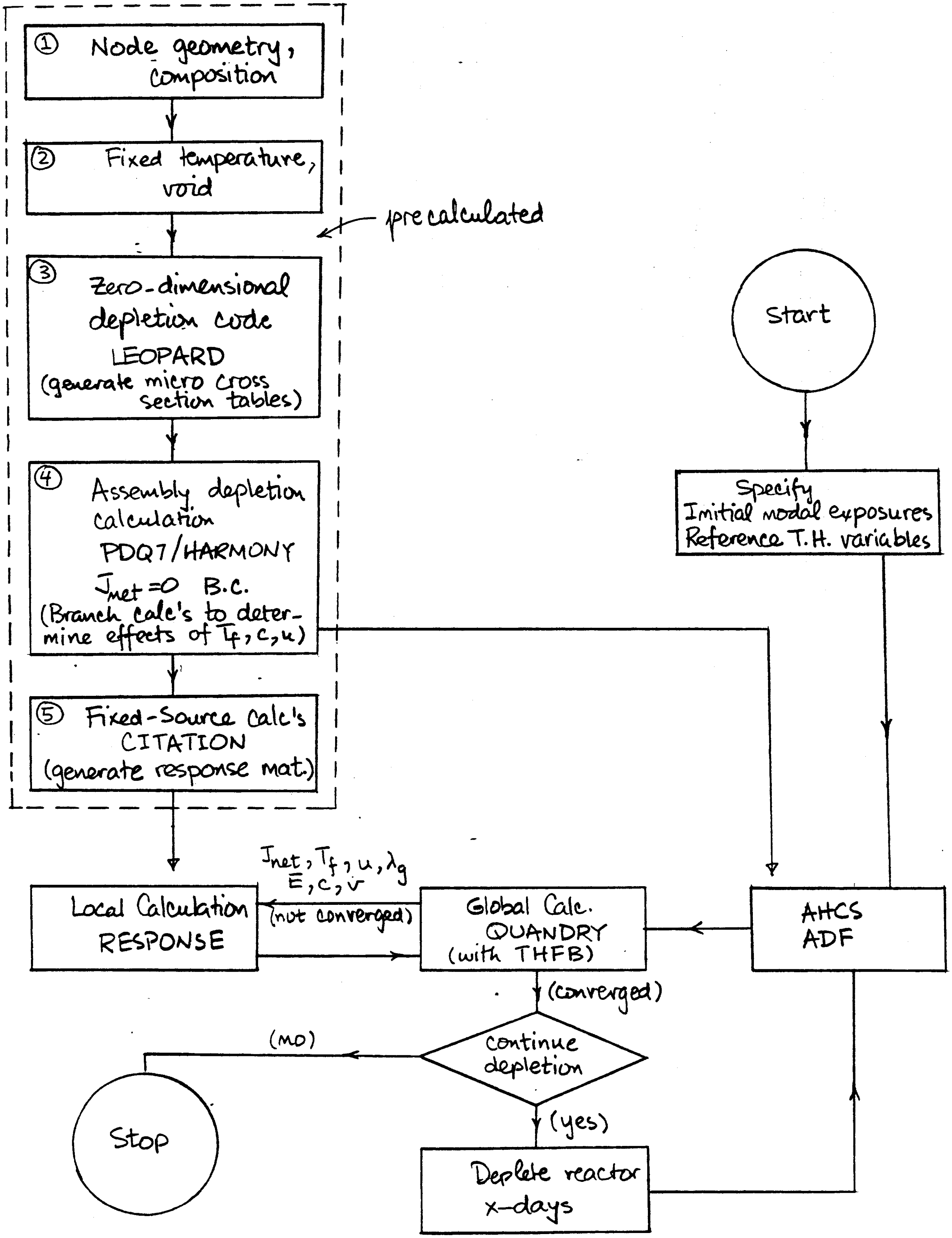
① Node geometry, composition
② Fixed temperature, void
precalculated
③ Zero-dimensional depletion code LEOPARD (generate micro cross section tables)
④ Assembly depletion calculation PDQ7/HARMONY $J_{net}=0$ B.C. (Branch calc's to determine effects of T_f, c, u)
⑤ Fixed-Source Calc's CITATION (generate response mat.)
Start
Specify Initial nodal exposures Reference T.H. variables
J_{net}, T_f, u, λ_g E, c, v
(not converged)
Local Calculation RESPONSE
Global Calc. QUANDRY (with THFB)
AHCS ADF
(converged)
continue depletion
(no)
(yes)
Stop
Deplete reactor x-days

Fig. 1. BWR depletion scheme for one operating cycle

This figure gives the required sequence of calculations, as well as some of the computer codes useful in their implementation.

In the "pretabulation" phase of the procedure, the assembly type may be varied in step 1, the coolant void fraction in step 2, and the global reactor eigenvalue (which must be assumed in obtaining the matrices) in step 5. Finally, branch calculations may be performed during step 4 at several exposures to determine variations in matrix elements with additional variables.

3.3 Numerical Testing

3.3.1 Simplifications of the Proposed Model. For the purposes of testing the overall QUANDRY depletion model and the response matrix method of assembly homogenization, it is clearly desirable to simplify considerably the procedure described in Sections 3.1 and 3.2. For example, since flux distributions in the axial direction are known to be rather smooth throughout life, attention can be focused on prediction of radial flux and power distributions for different x-y planes at fixed axial levels. Thus the depletion runs needed to test the overall model can be performed for two-dimensional systems. In addition, while a criticality search must in principle be performed to obtain the power distribution used to deplete the various assemblies, this complication need not be addressed in the present study. The cost associated with this search would be significant, and the overall method can be tested without recourse to it (provided that the same procedure is adopted for a reference solution). Thus the test runs would be performed with a continuously varying λ_g and no control blade history effects. Finally, if the fuel temperature variable is neglected, the ADF and AHCS will depend only on E, v, and u. (The response matrices will depend additionally on λ_g.) Consequently, the initial assembly depletion runs must be performed for different values of u, branch calculations would account for the effect of an instantaneous void u' different from u (=v), and response matrices must be tabulated for the different values of E, v, u, and λ_g.

3.3.2 Numerical Standard. A consistent numerical standard (reference solution) must be designed to test the proposed, simplified depletion method. Since the purpose of the study is the development of an improved depletion model and not the performance of depletion runs for an actual reactor), it is possible to use simple, few-assembly problems with imposed outer boundary currents (e.g. using albedo boundary conditions) to test the various procedures. For consistency, the reference solution should

(a) employ the same thermal-hydraulic feedback model as QUANDRY,

and (b) have the capability of depleting isotopes using the same depletion equations used in performing the initial assembly depletions.

Presently, it is not clear how to satisfy these constraints without revising QUANDRY so that it can solve isotope depletion equations and using QUANDRY fine-mesh solutions to deplete the assemblies as well as to provide the needed global fine-mesh reference. Thus it will be necessary either to interface QUANDRY with some existing depletion program, or to add a subroutine which will solve the isotope depletion equations and provide new macroscopic cross sections at the end of each depletion interval.

4. Response Matrix Behavior in Depletion Calculations

The success of the proposed depletion procedure will depend largely on the feasibility of determining accurately the response matrices for all node conditions of interest by interpolation. Thus, a study was performed to test the sensitivity of matrix elements to the two key variables in BWR depletion calculations, coolant void fraction v and exposure E. The cross section data required to compute the matrices were obtained from CASMO depletion runs performed by YAEC for the Vermont Yankee BWR bundle shown in Figure 2. Heterogeneous, macroscopic cross section data were thus obtained at exposures of 0, 5, 10, 20, and 30 MWD/kg for three different values of v (0, 0.4, 0.7). Variations of the two-group cross sections for three different fuel rod types, the gadolinium rods, and the water gaps with exposure for $v = 0.4$ are illustrated by Figs. 1-3 of Appendix 3.

4.1 Test Problem Description

In order to reduce the expense of performing the fixed-source calculations needed to obtain the response matrices, an assembly geometry different from that shown in Fig. 2 was used for matrix calculations. In particular, a 90° rotationally symmetric configuration was chosen (see Fig. 3) and thus only two fixed-source problems must be solved (for the unrodded case) to obtain the matrix elements[5]. Despite the assumption of a single width for the water gaps and a completely symmetric arrangement of compositions, this assembly still exhibits much of the heterogeneity found in actual BWR's. The

2.19 wt % U-235 bundle average

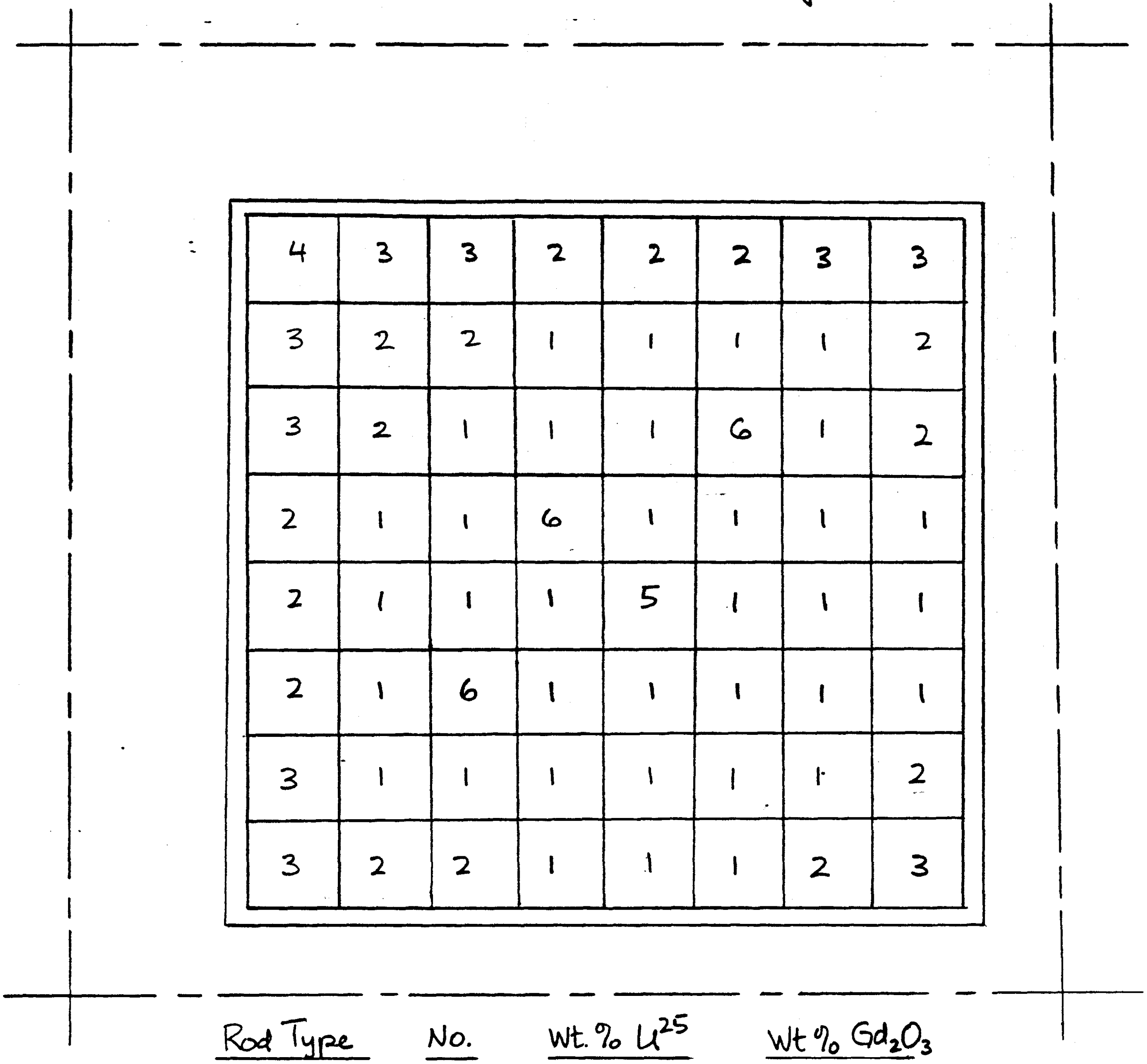

4	3	3	2	2	2	3	3
3	2	2	1	1	1	1	2
3	2	1	1	1	6	1	2
2	1	1	6	1	1	1	1
2	1	1	1	5	1	1	1
2	1	6	1	1	1	1	1
3	1	1	1	1	1	1	2
3	2	2	1	1	1	2	3

Rod Type	No.	Wt. % U^{25}	Wt % Gd_2O_3
1	35	2.50	0
2	15	1.90	0
3	9	1.49	0
4	1	1.18	0
5	1	Water tube	0
6	3	2.50	4.0

Fig. 2. Vermont Yankee Reload-2 Fuel Bundle

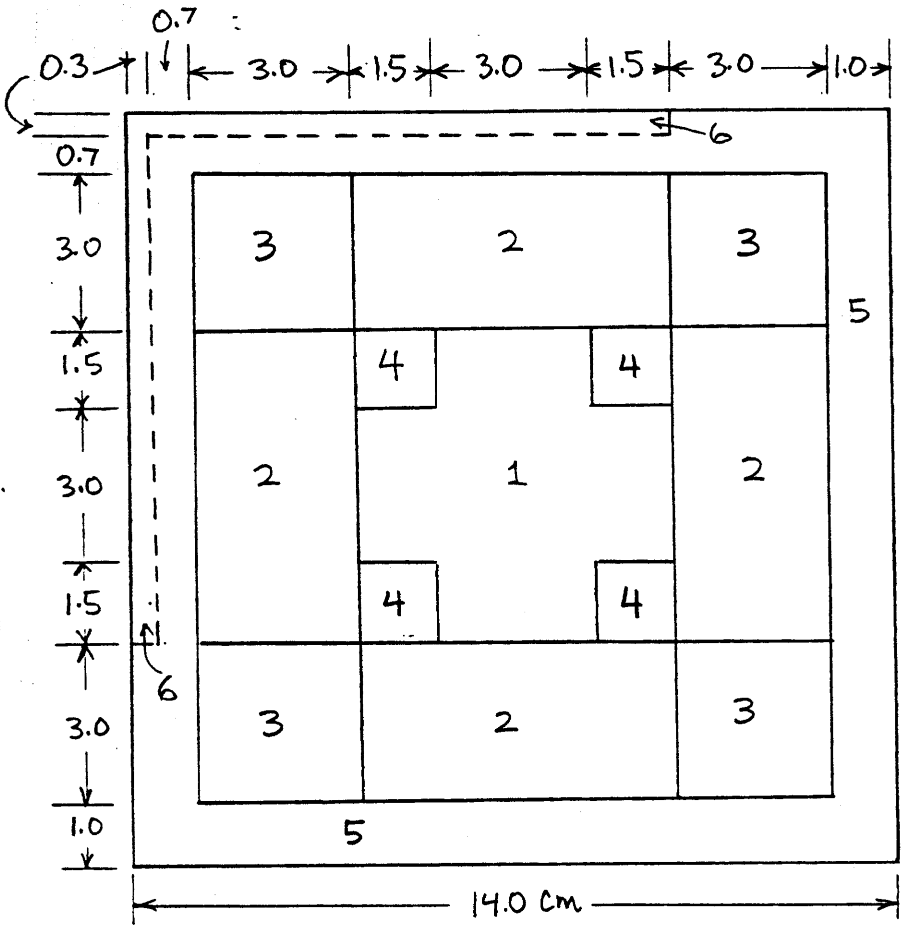
0.7
0.3
3.0
1.5
3.0
1.5
3.0
1.0
6
0.7
3.0
1.5
3.0
1.5
3.0
1.0
3
2
3
5
4
4
2
1
2
4
4
6
3
2
3
5
14.0 cm

Region	Composition
1	Type 1 fuel (2.5 w/o U^{25})
2	Type 2 fuel (1.9 w/o U^{25})
3	Type 3 fuel (1.49 w/o U^{25})
4	Gadolinium rod (2.5 w/o U^{25} + 4 w/o Gd_2O_3)
5	Water gap + fuel can
6 (unrodded)	"
6 (rodded)	Control rod

Fig. 3 BWR assembly used to test the effects of coolant void and exposure on response matrix elements

cross sections for the different regions were obtained directly from the CASMO runs, although their use for a slightly different geometry is not strictly correct. However the major effects of coolant void and exposure on the cross sections are well represented and permit evaluation of the variation of the response matrices with those variables.

4.2 Effects of Void and Exposure -- Matrix Singularity.

The matrices [R] and $[\hat{R}]$ (see Section 3.1) were computed for the following values of exposure and void:

Case (1) $E = 0$; $v = 0, 0.4, 0.7$
Case (2) $E = 5$ MWD/kg; $v = 0, 0.4, 0.7$
Case (3) $v = 0.4$; $E = 0, 5, 10, 20, 30$ MWD/kg

For the results of Case (1), it was seen that the variation of all the elements of [R] and $[\hat{R}]$ with v at E = 0 was extremely smooth (in fact, nearly linear)(*). However, when the nodal exposure was increased to 5 MWD/kg (Case (2)), the variation of the matrix elements with void was not smooth and was actually discontinuous (an explanation is provided below). Finally, for the conditions of Case (3), the matrix elements again did not exhibit a smooth behavior over the entire exposure range. As an example of this behavior, the observed variation of a typical element of [R], $R_{7,1}$, with exposure is shown in Figure 4; all the other elements of [R] and $[\hat{R}]$ varied in a very similar manner with E.

(*) The matrix [R] was not investigated in this study.

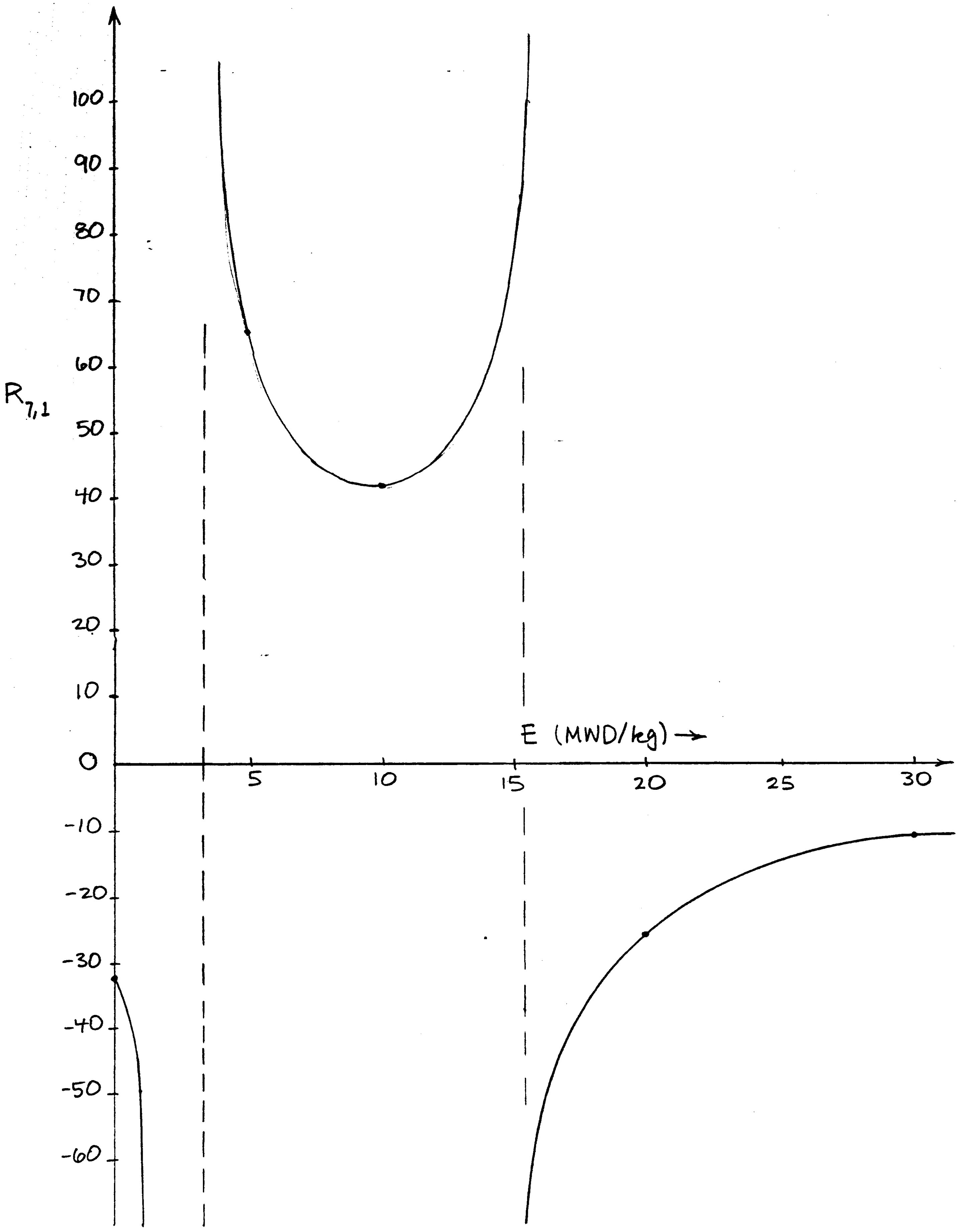

Fig. 4. Response matrix element as a function of exposure.

The discontinuous behavior of the matrix elements in Cases (2) and (3) is explained by the fact that the matrices [R] and $[\hat{R}]$ are based on imposed net surface-currents in the outward direction and are determined by fixed-source calculations in which a global reactor eigenvalue λ_g is assumed (λ_g was chosen to be unity in all calculations). When the k_∞ of the assembly is less than the assumed λ_g (i.e. the node is subcritical), the matrix elements (surface fluxes and interaction rates) are negative, whereas for $k_\infty > \lambda_g$, the matrix elements are positive. Furthermore, the elements in these two cases becomes increasingly negative and positive, respectively, as the assembly approaches the "critical" k_∞ (i.e. $k_\infty = \lambda_g = 1$). Thus the response matrix elements based on imposed net currents become infinite as the assembly passes through a critical state, a point that can be demonstrated rigorously for the simple case of a bare, homogeneous slab.

The results of Cases (1) through (3) may now be explained in terms of the variations of the assembly k_∞'s as the voids or exposure levels are varied. In Case (1), the node is subcritical at $E = 0$ and $v = 0$, and increasing v simply causes the node to become more subcritical. Thus the matrix elements are always negative and vary smoothly as v is varied. However, for $E = 5$ MWD/kg, the assembly is supercritical for $v = 0$, and increasing the void to 0.4 and 0.7 causes it to become subcritical. Thus at some void $0 < v < 0.4$, the assembly is exactly critical, and the matrix elements become infinite and vary discontinuously at this intermediate void. Finally, for Case (3), in which the void fraction was constant and exposure varied, it may be seen from Figure 4 that:

for $E \lesssim 3$ (*) , $k_\infty < 1$

for $3 < E \simeq 15$, $k_\infty > 1$

for $15 < E$, $k_\infty < 1$.

The assembly criticality at E = 3 and 15 causes the infinities in the matrix elements at these exposures.

(*) The units of exposure, MWD/kg, are dropped for simplicity.

5. Response Matrix Interpolation

It is unfortunate that the change in sign of node "reactivity" ($\equiv 1 - \frac{\lambda_g}{k_\alpha}$), i.e. matrix singularity, can result from the variation of a number of nodal variables. The discontinuous behavior of the matrices at critical values of the independent variables makes the interpolation of the matrix elements in depletion runs a non-trivial problem. Thus one of the primary objectives of this study was to determine and evaluate numerical methods applicable to interpolation of the response matrices when their behavior is discontinuous.

A possible alternative to the interpolation of the matrices $[R]$, $[\hat{R}]$, and $[\tilde{R}]$ is the interpolation of $[R]^{-1}$, $[P] \equiv [\hat{R}][R]^{-1}$, and $[Q] \equiv [\tilde{R}][R]^{-1}$. This latter set of matrices relates net currents and interaction rates to surface average fluxes via the relations

$$[J] = [R]^{-1} [\bar{\phi}^S] \tag{14}$$

$$[F] = [P] [\bar{\phi}^S] \tag{15}$$

$$[M] = [Q] [\bar{\phi}^S] \tag{16}$$

Since the matrices $[R]^{-1}$, $[P]$, and $[Q]$ represent net current and interaction rate "responses" to imposed surface fluxes, they remain finite when the node is critical and should vary continuously through the point $k_\infty = \lambda_g$. Another interpolation alternative is simply to interpolate the original matrices $[R]$, $[\hat{R}]$, and $[\tilde{R}]$ in a piece-wise manner over regions where their variation is smooth and continuous (i.e. where the node "reactivity" is of a constant sign).

Both interpolation alternatives were examined. Attention was focused on piecewise interpolation of the elements of [R] and interpolation of the elements of $[R]^{-1}$. Although the matrices $[\hat{R}]$, $[\tilde{R}]$, [P], and [Q] were not explicitly considered, interpolation techniques applicable to [R] would be suitable for $[\hat{R}]$ and $[\tilde{R}]$, while those applicable to $[R]^{-1}$ would be suitable for [P] and [Q]. Also, the exposure variable was arbitrarily chosen to test the two interpolation ideas.

5.1 Interpolation of [R] and $[R]^{-1}$

To obtain a sufficient number of data points to test the two interpolation alternatives, fixed-source calculations were performed at exposure intervals of 1 MWD/kg for $0 \leq E \leq 10$ and for a coolant void fraction of 0.4. The two-group heterogeneous cross sections used in these calculations were obtained by quadratic (for $0 \leq E \leq 5$) or bi-quadratic (for $5 \leq E \leq 10$) Lagrange interpolation of CASMO cross section data. Results of the fixed source calculations were used to compute the response matrices [R] and $[R]^{-1}$ as a function of E. The variation of a representative element of each of these matrices with exposure is shown in Figure 5. From part (a) of this figure, it may be seen that the elements of the matrix [R] become infinite for $E \simeq 3.3$; at this exposure, the node is exactly critical with $J \cdot n = 0$ boundary conditions. Fortunately, it is also seen that the matrix elements vary continuously and quite smoothly with exposure away from the troublesome point of singularity. Examination of

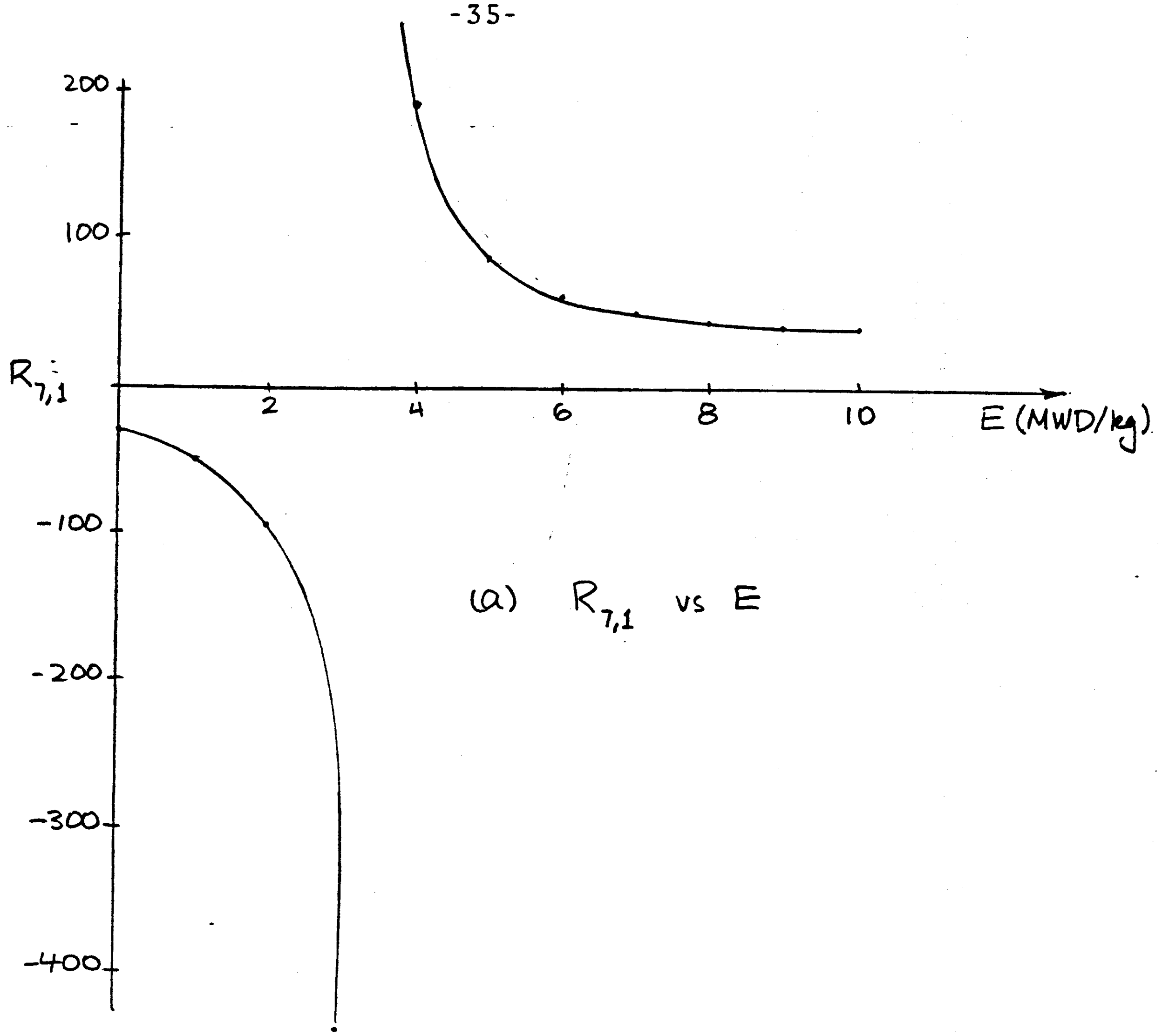

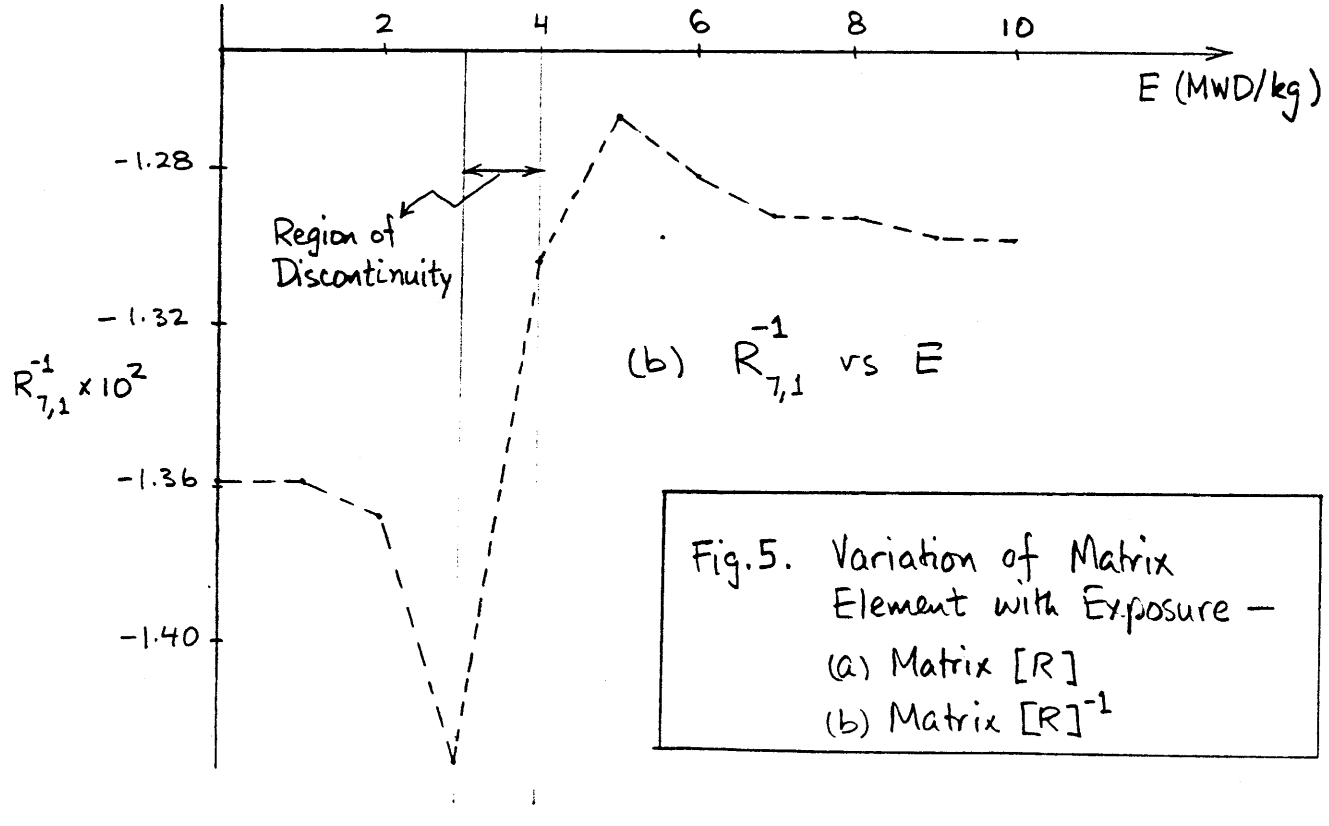

Fig. 5. Variation of Matrix Element with Exposure –
(a) Matrix [R]
(b) Matrix $[R]^{-1}$

Figure 5(b) reveals that the behavior of a typical element of $[R]^{-1}$ is not nearly as smooth, although the element remains finite for all values of E. Initially, numerical difficulties with the inversion of [R] were thought to be the cause of this irregular behavior. However, repetition of some of the inversions using (IBM) double-precision produced changes in the elements that are not discernible on the scale of Figure 5(b). Furthermore, the inversion of $[R]^{-1}$ to reobtain [R] yielded the original matrix to the last (7th) decimal place printed. Thus it appears that the elements of $[R]^{-1}$ do not vary smoothly when computed at reasonable exposure intervals, possibly because the collective behavior of all elements of [R] with the changing exposure level governs the variation of each element of $[R]^{-1}$. Since a given element of [R], R_{ij}, which is smaller than another element $R_{i'j'}$ at some E may become larger at a different E, the variation of $[R]^{-1}$ is somewhat complicated and not sufficiently smooth to permit interpolation by low-order polynomials.

Interpolation of the elements of [R] was tested using the formula

$$R_{i,j}(E) = C\left[(E-E^*)^3 + b(E-E^*)^2 + a(E-E^*)\right]^{-1} \tag{17}$$

where $R_{i,j}(E)$ ≡ the (i,j) element of [R] at exposure E

E^* ≡ the exposure for which $R_{i,j} \to \infty$

a,b,c ≡ constants determined by fitting Eq. (17) to known values of $R_{i,j}$ at three different values of E.

With E^* = 3.3, and with the constants a, b and c determined using the calculated values of $R_{7,1}$ at E = 0, 1, 2 [see Figure 5(a)], $R_{7,1}(E=3)$ was predicted with an error of only 1.8%. The same value of E^* and a, b, c obtained from data at E = 5, 6, 7 yielded $R_{7,1}(E=4)$ with an error of -6.6% and $R_{7,1}(E=8)$ with an error of -3.6%. Since all these cases represent extrapolations, and since the value of E^* is not known exactly, these errors are actually quite small. Errors of this magnitude may be acceptable if the accuracy of the local (response matrix) calculations in the proposed BWR depletion method is not extremely sensitive to small errors in the matrix elements in the neighborhood of a discontinuity.

6. Sensitivity of Local Calculations to Response Matrix Errors

The sensitivity of the results of local response matrix calculations (i.e. HCS and DF) to errors in extrapolated matrix elements about the point of matrix singularity is an important consideration. This sensitivity was tested for the simple 3-node by 3-node problem shown in Figure 6. The geometric detail of each of these nodes is that of the unrodded configuration of the BWR assembly shown in Figure 3, but the various nodes are characterized by different levels of exposure. The coolant void fraction and the fuel temperature are the same for all the nodes, and $\underline{J}\cdot\underline{n} = 0$ boundary conditions are imposed on the outer boundary of the nine-node cluster.

Assembly calculations were first performed for each node type to obtain its k_∞ as well as assembly discontinuity factors ADF and assembly homogenized cross sections AHCS. Using the ADF and AHCS, the global homogeneous problem was solved to obtain net surface currents to be used in local five-node, two-segment response matrix calculations. (It should be noted that for E=3 (MWD/kg), the nodal k_∞ differed from the ADF λ by less than 0.5%, and thus its matrix elements were quite large in magnitude.) The local calculations were performed twice, once with the "exact" matrices (precomputed by fixed-source calculations) used for the E=3 nodes and once with approximate matrices extrapolated to E=3 (using Eq. (17)) from fixed-source results at E=0, 1, and 2. In both cases, the "exact" matrices were used for the E=0 and E=10 nodes. Finally, the global problem solution was repeated using the HCS and DF

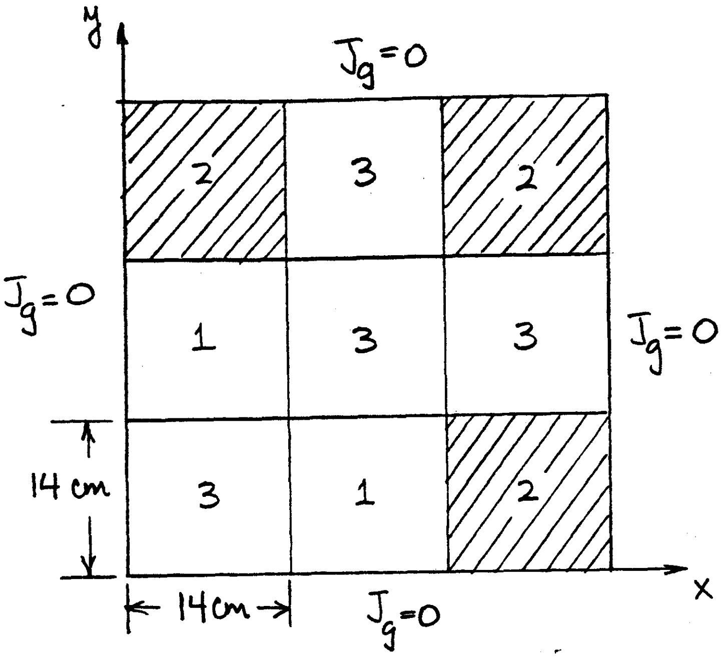
y
Jg=0
2
3
2
Jg=0
1
3
3
Jg=0
14 cm
3
1
2
x
14cm
Jg=0

Node	E (MWD/kg)	k_∞
1	0	0.9473
2	3	0.9952
3	10	1.0392.

$v = 0.4$ for all nodes

Fig. 6. Problem to test sensitivity of local/global calculations to response matrix errors. The nodes labeled 2 are nearly critical.

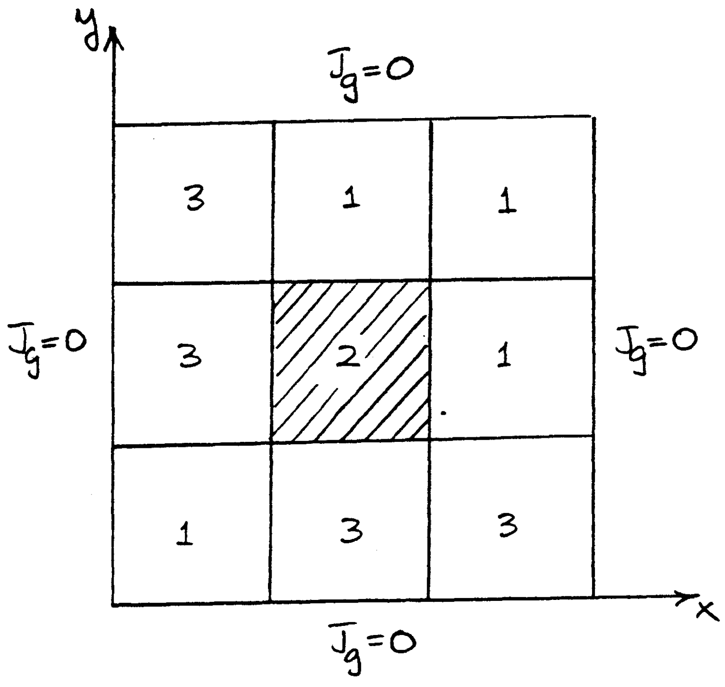
y
Jg=0
3
1
1
Jg=0
3
2
1
Jg=0
1
3
3
x
Jg=0

Node types 1, 2, and 3 same as Fig. 6

Fig 7. Problem to test accuracy of interpolation of homogenized cross sections and discontinuity factors "across" point of response matrix singularity

updated in each of these local calculations. Results of the entire problem are summarized in Table 1 and indicate that although all the matrix elements for E=3 were in error by about 2%, the resultant errors in HCS, DF, power, and eigenvalue were all less than 0.15%. Thus it appears that the error in the response matrix elements of the nodes that are nearly critical leads to negligible errors in the results for the local calculations.

Table 1. Comparison of center-node flux, power, homogenized cross sections and discontinuity factors and the global eigenvalue for the problem shown in Fig. 6.

			Second Global Calculation		
		ADF	Response Matrices Computed	Response Matrices Extrapolated	(% error)
λ		1.00023	1.00079	1.00078	(.02)
$P/\bar{P}$		1.002	1.002	1.002	
ϕ	ϕ_1	20.94	20.92	20.92	
	ϕ_2	5.756	5.785	5.788	(.05)
HCS	D_1	1.669	1.669	1.669	
	$\Sigma_{t1} \times 10^2$	2.147	2.147	2.147	
	$\Sigma_{21} \times 10^2$	1.462	1.461	1.462	(.06)
	$\nu\Sigma_{f1} \times 10^3$	3.928	3.929	3.929	
	$\Sigma_{f1} \times 10^3$	1.504	1.504	1.504	
	$D_2 \times 10^1$	4.217	4.210	4.211	(.02)
	$\Sigma_{t2} \times 10^2$	5.341	5.310	5.307	(.06)
	$\nu\Sigma_{f2} \times 10^2$	6.374	6.345	6.338	(.11)
	$\Sigma_{f2} \times 10^2$	2.533	2.521	2.520	(.03)
DF(*)	XL1 = YL1	0.9698	0.9726	0.9734	(.08)
	XL2 = YL2	1.4091	1.408	1.409	(.07)
	XU1 = YU1	0.9698	0.9664	0.9658	(.06)
	XU2 = YU2	1.4091	1.403	1.401	(.14)

(*) XL1 = x-lower group 1
XL2 = x-lower group 2
XU1 = x-upper group 1
XU2 = x-upper group 2

because of diagonal symmetry, y-direction discontinuity factors are the same

7. An Alternate Interpolation Strategy

It is unfortunate that use of Eq. (17) to interpolate matrix elements requires at least three data points on either side of a discontinuity, as well as an accurate knowledge of the value of the independent variable at which the matrices are singular. In view of the fact that several variables can cause matrix singularity, the number of response matrices that would have to be generated and stored becomes enormous. Thus it may be advantageous to utilize an alternate interpolation scheme in which the HCS and DF themselves are interpolated instead of the matrix elements. In this method, a number of different local calculations with response matrices appropriate to values of some independent variable x surrounding the value at which the HCS and DF are needed would be performed. Results of these local calculations can then be interpolated to yield the desired HCS and DF at the correct value of x. The success of this method obviously depends on how smoothly the nodal HCS and DF vary through a point of assembly criticality.

To test the feasibility of interpolation of the HCS and DF "across" a point where the matrices are singular, the problem shown in Fig. 7 was considered. For this problem the global, homogeneous calculation using the ADF and AHCS yielded $\lambda = 0.9955$ which is very close to the k_∞ of the E = 3 node, 0.9952. The local five-node response matrix calculation was performed three times with different response matrices assigned to the center node (E=3). The correct E=3 matrices were used, as well as matrices for exposures surrounding E=3, namely E=2 and E=4. The matrix elements are singular at

E = 3.3 and thus have differing signs and large magnitudes at E=3 and E=4. The DF and HCS computed for the cases in which the E=2 and E=4 matrices were used were averaged and compared with the correct E=3 results and the ADF results. This comparison is presented in Table 2, from which it may be seen that the averaged results match quite closely the correct results, even though the response matrix elements are infinite and discontinuous at an exposure between E=3 and E=4.

Although the outcome of this problem indicates that it is indeed possible to interpolate the HCS and DF across the point of matrix discontinuity, the accuracy that was demonstrated may have been largely due to the absence of any void or control mismatch among the various nodes (only the nodal exposures were different). This uniformity of void fraction caused the fast to thermal current ratios J_1/J_2 at the node boundaries to approach an asymptotic value. Thus a more difficult three-node by three-node problem was developed in which three of the nodes were characterized by $v = 0$, and the remaining ones by $v = 40\%$. This problem is shown in Fig. 8.

As expected, the global calculation using assembly discontinuity factors ADF yielded widely differing J_1/J_2 over the interior surfaces of the nine-node cluster. Furthermore, the ADF λ of 0.99773 was very close to the k_∞ of the center node, causing its matrix elements to be very large in magnitude. Following the ADF calculation, one-node, one-segment local response matrix calculations were performed three times -- first with the center-node matrices at the correct exposure (E = 3) and then with matrices at surrounding

Table 2. Comparison of the center-mode discontinuity factors and homogenized cross sections for the ADF calculation and two global calculations based on use of different response matrices for the center node. (see Fig. 7 for the problem description).

	ADF	Second Global Calculation		
		Using correct (E=3) response matrices for center mode	Average of results using E=2 and E=4 matrices (% error)	
HCS:				
D_1	1.669	1.669	1.669	
$\Sigma_{t1} \times 10^2$	2.147	2.147	2.148	(.05)
$\Sigma_{21} \times 10^2$	1.462	1.461	1.462	(.07)
$\nu\Sigma_{f1} \times 10^3$	3.928	3.929	3.929	
$\Sigma_{f1} \times 10^3$	1.504	1.504	1.504	
$D_2 \times 10^1$	4.217	4.210	4.211	(.02)
$\Sigma_{t2} \times 10^2$	5.341	5.310	5.303	(.13)
$\nu\Sigma_{f2} \times 10^2$	6.374	6.345	6.332	(0.2)
$\Sigma_{f2} \times 10^2$	2.533	2.521	2.517	(0.2)
DF$^{(*)}$:				
XL1	0.9698	0.9406	0.9399	(.07)
XL2	1.4091	1.373	1.373	
XU1	0.9698	1.002	1.006	(0.4)
XU2	1.4091	1.440	1.444	(0.3)

(*) See table 1

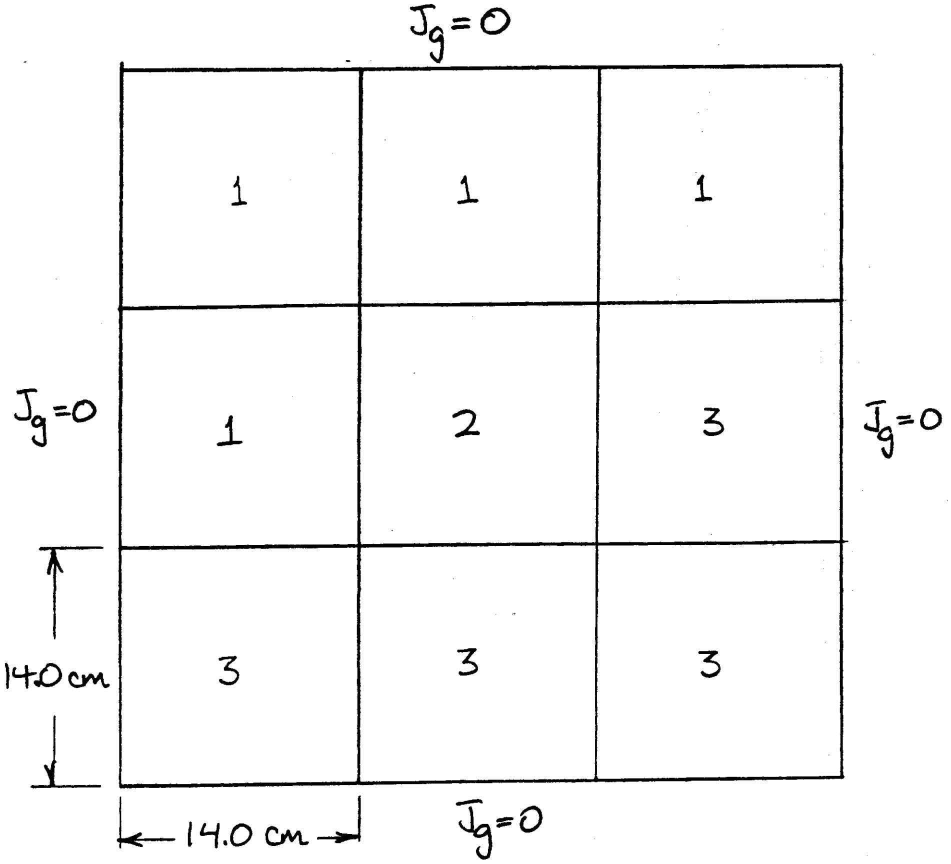

$J_g=0$
1
1
1
$J_g=0$
1
2
3
$J_g=0$
14.0 cm
3
3
3
14.0 cm
$J_g=0$

Assembly Type	Exposure, E (MWD/kg)	Void, v	k_∞
1	0	40	0.9473
2	3	40	0.9952
3	5	0	1.0326

Fig. 8. Problem to test accuracy of interpolation of homogenized cross sections and discontinuity factors "across" point of matrix singularity.

exposures (E = 2 and E = 4). Since the matrix elements are singular at E ≃ 3.3, matrices of differing signs and large magnitudes were assigned to the center node in the three different local calculations. A comparison of the HCS and DF obtained by using the correct E=3 matrices to those determined by averaging the E=2 and E=4 results is presented in Table 3. From this table it is clear that the simple averaging of local calculation results (i.e. the HCS and DF) is much less accurate for this problem, in which a significant void mismatch exists. For example, one of the averaged DF's was in error by more than 20%.

To determine the effect of the errors in HCS and DF on the ensuing global calculation, the averaged values were used in another global QUANDRY run. The resulting eigenvalue and center-node fluxes and power were compared with the correct values (determined using the correct E=3 matrices for the center node in the local calculations) and with the ADF values. This comparison is presented in Table 4 and indicates that even with the large DF errors, the resultant errors in the global solution were very small and still represented an improvement over the ADF results.

The results of these test problems are very encouraging because they indicate that although a matrix element cannot be interpolated using known values on different sides of a singularity, the desired HCS and DF themselves can be found in this manner.

	ADF.	Second Global Calculation			
		Correct Response Matrices for Node 2	Response Matrices E=2	Response Matrices E=4	Average of E=2 & E=4 (% error)
D_1	1.669	1.670	1.671	1.670	1.670 (0)
$\Sigma_{t1}\times10^2$	2.147	2.145	2.123	2.150	2.137 (0.4)
$\Sigma_{21}\times10^2$	1.462	1.457	1.418	1.463	1.441 (1.1)
$\nu\Sigma_{f1}\times10^3$	3.928	3.944	4.132	3.864	3.998 (1.4)
$\Sigma_{f1}\times10^3$	1.504	1.510	1.589	1.473	1.531 (1.4)
$D_2\times10^1$	4.217	4.186	4.103	4.274	4.189 (0.1)
$\Sigma_{t2}\times10^2$	5.341	5.206	4.812	5.569	5.191 (0.3)
Σ_{12}	0	0	0	0	0 -
$\nu\Sigma_{f2}\times10^2$	6.374	6.217	5.621	6.812	6.217 (0)
$\Sigma_{f2}\times10^2$	2.533	2.470	2.257	2.682	2.470 (0)
DF :					
XL1	0.9698	0.9631	0.8095	0.9748	0.8922 (7.4)
XL2	1.4091	1.345	1.066	1.529	1.298 (3.5)
XU1	0.9698	0.9636	0.9391	0.9778	0.9585 (0.6)
XU2	1.4091	1.376	1.304	1.543	1.424 (3.5)
YL1	0.9698	0.9596	0.9271	0.9903	0.9587 (0.1)
YL2	1.4091	1.357	1.266	2.017	1.642 (21)
YU1	0.9698	0.9684	0.9996	0.9666	0.9831 (1.5)
YU2	1.4091	1.369	1.029	1.471	1.250 (8.7)

Table 3. Comparison of center-mode homogenized cross sections and discontinuity factors for the ADF calculation and the subsequent global calculation based on use of different response matrices for the center mode in the local calculations.

	ADF (% error)	Using Correct HCS & DF	Using Averaged HCS & DF (% error)
λ	0.99773 (0.17)	0.99942	0.99963 (0.02)
$P/\bar{P}$	0.9173 (0.63)	0.9231	0.9209 (0.23)
Φ_1	18.30 (0.54)	18.40	18.64 (1.30)
Φ_2	5.321 (3.03)	5.487	5.441 (0.84)

Table 4. Comparison of global eigenvalue and center mode group fluxes and power for different global solutions.

8. Summary, Conclusions, and Recommendations

An overall strategy for performing BWR depletions using the nodal code QUANDRY and response matrix methods for assembly homogenization has been outlined. A few ideas useful for testing the various procedures in a consistent manner were also presented. The problem of interpolating response matrices based on net currents was found to be challenging because of the singularity of the matrix elements when the value of some nodal property causes the node to be critical.

A number of interpolation techniques were examined. It was shown that interpolation of the inverted response matrices (i.e. matrices based on average surface fluxes) is not a practical alternative. An interpolation formula suitable for piece-wise interpolation of the response matrices (Eq. (17)) was shown to yield the various elements with good accuracy even at node conditions very close to critical. The resultant errors in matrix elements were shown to be quite unimportant as far as their effects on the HCS and DF are concerned. Unfortunately, use of a formula of this type would be impractical when multi-dimensional (or a series of one-dimensional) interpolations are needed, since the formula requires at least three points on either side of every point of discontinuity. Thus the number of matrix elements that must be calculated and stored may become unacceptably large.

It was also demonstrated in this study that it is feasible to interpolate HCS and DF computed by the use of (incorrect) matrices at conditions surrounding the desired ones (for which matrices cannot be interpolated by standard methods due to singular behavior). However, this method was successful partly because known (i.e. pre-computed) matrices were available at conditions very close to critical. Moreover, this interpolation method was implemented by running the entire code RESPONSE twice (with matrices corresponding to conditions surrounding the actual conditions of the critical nodes), and thus local calculations were needlessly repeated for nodes not close to criticality. Clearly, it would be more practical to modify the code RESPONSE so that local calculations would be repeated only for nearly critical nodes.

Most probably, a combination of the two investigated interpolation strategies will be needed to obtain sufficiently accurate values of the desired nodal DF and HCS for arbitrary nodal conditions.

Obviously, a great deal remains to be accomplished in both formulation and solution of the depletion problem. Presently, the most immediate concerns appear to be:

i) Modification of QUANDRY to permit solution of isotope depletion equations and calculation of macroscopic cross sections over life. This may be accomplished by interfacing QUANDRY with a simple existing depletion program.

ii) Design of a simple (e.g. 3-assembly by 3-assembly, two-dimensional global problem with albedo boundary conditions to obtain a reference depletion run against which the proposed depletion methods can be tested.

iii) Determination of a suitable method applicable to the multi-dimensional interpolation of nodal response matrices when the variation of any of the nodal properties may cause criticality (i.e. matrix singularity). It should be noted, however, that the concern here is not that a node will be exactly critical during the course of a depletion calculation (this is extremely unlikely); the problem is rather that of obtaining nodal homogenization parameters when data required for interpolation exist on "different sides" of a singularity.

iv) Examination of the accuracy with which local power peaks can be predicted over life with the response matrix methods that have been developed to date.

The last two of these four items will probably have the biggest impact on the success of the proposed depletion model. However, there is little reason to doubt that the various questions can be resolved satisfactorily, and that the computational advantages of using QUANDRY and the response matrix technique of assembly homogenization for static calculations will also be realized in depletion calculations.

9. References

1. D.L. Delp, et al., "Flare, A Three-Dimensional Boiling Water Reactor Simulator," GEAP-4598, General Electric Company (1964).

2. K.S. Smith, "An Analytic Nodal Method for Solving the Two-Group, Multidimensional, Static and Transient Neutron Diffusion Equations," S.M. Thesis, M.I.T., Cambridge, Mass. (March 1979).

3. K.S. Smith, "Spatial Homogenization Methods for Light Water Reactor Analysis," Ph.D. Thesis, M.I.T., Cambridge, Mass (June 1980).

4. K. Koebke, "A New Approach to Homogenization and Group Condensation," Paper presented to the IAEA Technical Committee Meeting on Homogenization Methods in Reactor Physics, Lugano, Switzerland (November 1978).

5. A.Y.C. Cheng, "Homogenization of BWR Assemblies by Response Matrix Methods," Ph.D. Thesis, M.I.T., Cambridge, Mass (May 1981).

6. E.G. Adensam, et al., "Computer Methods for Utility-Reactor Physics Analysis," Reactor and Fuel Processing Technology, 12, 2 (Spring 1969).

7. A.F. Henry, Nuclear-Reactor Analysis, M.I.T. Press, Cambridge, Mass., 1975.

8. E.P. Wigner and J.E. Wilkins, Jr., "Effects of the Temperature of the Moderator on the Velocity Distribution of Neutrons With Numerical Calculations for H as Moderator," USAEC Report AECD-2275 (1944).

9. R.F. Barry, "LEOPARD -- A Spectrum Dependent Non-Spatial Depletion Code," WCAP-3269-26 (September 1963).

10. W.R. Cobb, et al., "EPRI-CELL Code Description," Part II, Chap. 5, ARMP System Documentation Structure (1976).

11. C.G. Poncelet, "LASER -- A Depletion Program for Lattice Calculations Based on MUFT and THERMOS," USAEC Report WCAP-6073, Westinghouse Electric Corporation (April 1966).

12. T.R. England, "CINDER -- A One-Point Depletion and Fission Product Program," USAEC Report WAPD-TM-334, Westinghouse Electric Corporation (August 1962, revised June 1964).

13. A.F. Henry, "A Theoretical Method for Determining the Worth of Control Rods," WAPD-218 (1959).

14. P. Lemberg, "The Rodworth Code -- A Blackness Theory Calculation of Effective Few Group Diffusion Theory Parameters for Cruciform and RCC Shaped Control Rods," UNC-5228 (1968).

15. M. Edenius and A. Ahlin, "MICBURN -- Microscopic Burnup in Gadolinia Pins," Part II, Chap. 7, ARMP System Documentation Structure (1975).

16. W.R. Caldwell, "PDQ-7 Reference Manual," WAPD-TM-678 (1967).

17. T.B. Fowler, et al., "Nuclear Reactor Core Analysis Code: CITATION," Revision 2, ORNL-TM-2496, Oak Ridge National Laboratory (July 1971).

18. A. Johnsson et al., "Verification of a Fuel Assembly Spectrum Code Based on Integral Transport Theory," T1S-5815, Paper Presented at the ANS Annual Meeting (June 1978).

Edenius

19. A. Ahlin and M. Edenius,"The Collision Probability Module EPRI-CPM," Part II, Chap. 6, ARMP System Documentation Structure (1976).

20. YAEC draft, "CASMO Description and Verification," (October 1980).

21. M.J. Driscoll, Lecture Notes, M.I.T. Subject 22.35 (Spring 1981).

22. P.N. Ontko, "FLARE G -- A Three-Dimensional Reactor Simulator," S.M. Thesis, M.I.T., Cambridge, Mass. (February 1971).

23. L. Goldstein et al., "Calculation of Fuel Cycle Burnup and Power Distribution of the Dresden I Reactor With the TRILUX Fuel Management Program," Trans. Am. Nucl. Soc. 10, 1, p 300 (June 1967).

24. S. Børresen, "Characteristics and Performance of the 3-D LWR Simulator PRESTO," Trans. Am. Nucl. Soc., 15, p 956 (1972).

25. D.M. VerPlanck and D.R. Ferguson, "SIMULATE, Reactor Simulator Code, User's Manual," YAEC (1972); revision (September 1975).

26. E.E. Pilat and D.M. VerPlanck, Personal Communication (Fall 1980).

27. J.M. Holzer, "User's Manual -- QUANDRY Version 1 for the CDC CYBER 175," YAEC-1212 (March 1980).

Appendix 1. Response Matrix Generation

A flow diagram illustrating the various calculational steps and the computer codes used to compute the response matrices [R] and $[\hat{R}]$ is shown in Fig. A1.1. This procedure is also outlined in Table A1.1, along with some of the details of running the code CITATION. A sample CITATION input data file is given in Table A1.2.

The different input and output device numbers needed to execute the various programs are given in Table A1.3. The correspondence between these device numbers and actual input and output files are presented in Table A1.4. Finally, Table A1.5 gives the input data (File 37) required to run the different codes.

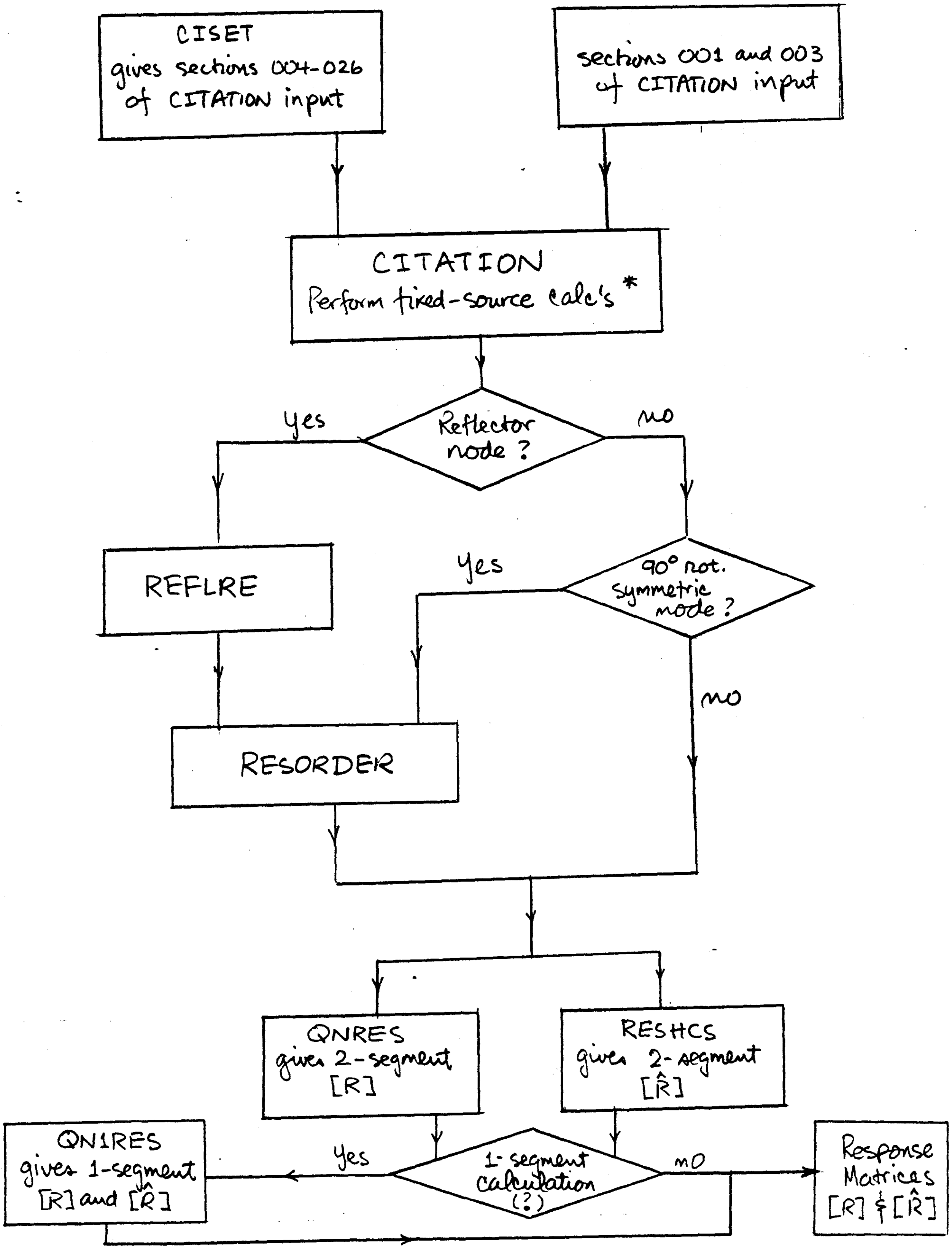
CISET
gives sections 004-026
of CITATION input
sections 001 and 003
of CITATION input
CITATION
Perform fixed-source calc's *
yes
Reflector
node ?
no
REFLRE
yes
90° rot.
symmetric
mode ?
no
RESORDER
QNRES
gives 2-segment
[R]
RESHCS
gives 2-segment
[R̂]
QN1RES
gives 1-segment
[R] and [R̂]
yes
1-segment
calculation
(?)
no
Response
Matrices
[R] & [R̂]

*Two calculations needed if mode is 90° rotationally symmetric
Eight calculations needed if mode is diagonally symmetric

Fig. A1.1 Response matrix generation procedure

Table A1.1

Procedures (for Preparation of Running 'RESPONSE')

1. Run CISET - prepare input file for fixed source calculation.
2. Run CITATION - solve fixed source problem.
    - A. If no on-line module, run NEWLOAD VS1JOB - create on-line module and solve the fixed source problem.
      NOTE: the time limit in NEWLOAD is not enough for 8 case^s of 29x29.
      CHANGE; a. NEWLOAD VS1JOB (CITATION LOAD40KC) (1 place)
      b. CITATION GOCARDS (FT44F001 DSN=?) (1 place)
      c. CITATION FORTRAN (XTFLUX(??) & KG=1) (7 places)
      KG=1,2 for all type and case except for reflector and source in 2nd group, then KG=1,1
    - B. If on-line module exists, run CITATION VS1JOB - solve fixed source problem.
      NOTE: time limit
      CHANGE: a. CITATION VS1JOB (FT44F001 DSN=?)
      (CITATION LOAD 40KC) (2 places)
3. If it is reflector, run REFLRE - create CL symmetric file.
4. If it is CL symmetric, run RESORDER - create diagonal^{ly} symmetric file.
5. Run QNRES - generate 2-segment R, (ϕ=RJ)
   $[R]$, $([\bar{\phi}^S] = [R][J])$
6. Run RESHCS - generate 2-segment R', (IR=R'J)
   $[\hat{R}]$, $([F] = [\hat{R}][J])$
7. Run QN1RES - generate 1-segment R and R' (ϕ = RJ, IR = R'J)

$\phi \equiv [\bar{\phi}^s]$
$J \equiv [J]$
$R \equiv [R]$
$IR \equiv [F]$
$R' \equiv [\hat{R}]$

	1	2	3	6	34	35	36	37	38	39	50*NLSOM	50+NST+NLSCOM	50+2*NST+NLSCOM
CISET				x				x	x*	x		x	
REFLRE	x	x	x					x					
RESORDER	x						x	x					
QNRES				x			x	x	x*		x		
RESHCS				x			x	x					x
QN1RES				x	x	x		x			x	x	x

* if ISHA≠1

ISHA = 1 for a flat current dist^n
≠ 1 for other shapes

(only ISHA = 1 is presently available)

NST = no. of node types in core

NLSCOM = nodal index
(NLSCOM = 1, ..., NST)

Table A1.3 Input and Output Device Numbers Needed to Run the Codes Used in the Response Matrix Generation Process and to Perform the Global/Local Iteration

LE NO.	DESCRIPTIONS	DISK	FILE MODE	RECFM	LRECL	BLKSIZE
1	if reflector Rℓ℄ SYM. FLUX. D.P. (L-R, T-B) (J, I, G) I goes first	DISK.	D	VBS	4096	4096
1	if not reflector Rℓ℄ SYM. FLUX. D.P. "	x1 DSN	-	—	—	—
2	reflecter, source in 1st group Rℓ℄ SYM FLUX. D.P. "	x1 DSN	-	-	-	—
3	reflector, source in 2nd group Rℓ℄ SYM FLUX. D.P. "	x1 DSN	-	-	—	—
6	PRINTOUT	DISK	E	F	132	132
34	1-segment R′ (IR=R′J) s.p. (J,I) J goes first	DISK	D	VBS	4096	4096
35	1-segment R (φ=RJ) s.p. "	DISK	D	VBS	4096	4096
36	if not R&℄ SYM. flux, D.P. (L-R, T-B) (J, I, G) I goes first	x1 DSN	-	-	-	-
36	if R&℄ SYM., flux, D.P. "	DISK	D	VBS	4096	4096
37	input data file	DISK	A	-	—	—
38	shaped flux file D.P. (L-R, T-B), (J, I, G) I goes first needed only if ISHA ≠ 1	DISK	D	VBS	4096	4096
39	Section 004-026 for CITATION INPUT	DISK	A	—	—	—
50tHILSCOM	2-segment response matrix R (J, I) φ=RJ s.p. J goes first	DISK	D	VBS	4096	4096
50tNST FNLSCOM	distributions, s.p.	DISK	D	-	—	—
50t2ANST FNLSCOM	2-Segment R′ (IR=R′J) (J, I) s.p. J goes first	DISK	D	VBS	4096	4096

Table A1.4. File definitions needed for generating response matrices and for using the Code RESPONSE

Table A1.5 Input Data Used in Response Matrix Generation

(FILE 37)

Card 1	(6X, 11I6)	
1-6	blank	
7-12	NLX	no. of meshes in X-dir.
13-18	NLY	no. of meshes in Y-dir.
19-24	NG	no. of groups
25-30	NSLX	X-dir. segment position (L→R)
31-36	NSLY	Y-dir. segment position (B→T)
37-42	ISYM	diagonal symmetry (LT→RB) 1→SYM 2→NOT SYM
43-48	NST	no. of nodal types in the core
49-54	NLSCOM	no. of nodal type of this subassembly
55-60	NLTCOM	no. of mesh types
61-66	ISHA	current distributions 1→flat ≠1→others
67-72	NSEG	no. of segments
Card 2	(12X, 5E12.6)	
1-12	blank	
13-24	XYI	sign convention = 1.00 if $\lambda_g > \kappa_\infty$ =-1.00 if $\lambda_g < \kappa_\infty$
25-36	XLAM	(estimated global eigenvalue)
Card 3	(12X, 5E12.6)	
1-12	blank	
13-24 ⋮ 61-72	DHX(1) ⋮ DHX(NLX)	X-dir. mesh size (L→R) use as many cards as needed

Table A1.5 (continued)

Card 4	(12X, 5E12.6)	
1-12	blank	
13-24	DHY(1)	Y-dir mesh size (B→T) use as many cards as needed
61-72	DHY(NLY)	
Card 5	(6X, 11I6)	
1-6	blank	
7-12	NLCOMP(NLY,NLX)	mesh map (L→R) (T→B) X-dir goes first use as many cards as needed in each dir., initiate a new card for different Y
67-72		
Card 6	(12X, 5E12.6)	
1-12	blank	
13-24	NLS(5*NG, NLTCOM)	$1/D_g$, Σ_{T_g}, $\Sigma_{g'g}(g' \neq g)$, $\nu\Sigma_{fg}$, Σ_{fg} first fast group then thermal group (not needed if NG=1) Remember $\overline{\nu\Sigma_{fg}} \neq \overline{\nu}\cdot\overline{\Sigma}_{fg}$ then different com- position
61-72		

Appendix 2. The Global/Local Iteration

In the global/local iteration, the global calculation is performed using QUANDRY, while local calculations for the various nodes are performed by the code RESPONSE. Input needed to run QUANDRY is described in Reference 27, while the input data used by RESPONSE is given in Table A2.1. Table A2.2 gives the correspondence between input and output device numbers and the different input and output files employed in carrying out the QUANDRY/ RESPONSE iteration.

Table A2.1 Input Data for RESPONSE

(FILE 50)

Card 0	(6I2, 2X, 19A4)	
1-2	NC = 0	card type
3-4	blank	
5-80	Alphanumeric title	
Card 1	(I2, 4X, 11I6)	
1-2	NC = 1	card type
3-6	blank	
7-12	NX	no. of nodes in X-dir.
13-18	NY	no. of nodes in Y-dir.
19-24	NG	no. of groups
25-30	NLOC	no. of nodes in local problems (1 or 5)
31-36	NSEG	no. of segments on the surfaces of each node (1 or 2)
37-42	NQND	current distribution between segments, useful only if NSEG=2 1-flat (0.5) ≠1-others
43-48	NST	no. of nodal types in the core
49-54		
Card 2	(I2, 4X, 11I6)	
1-2	NC = 2	card type
3-6	blank	
7-12	ICORE	container array size in D.P. words (0-code calculates)
13-18	IBPONT	BPOINTER print flag 0-NONE 2-ALLOCATIONS
19-24	NAT[+]	accuracy test 0-NO 6-IMSL TEST 0 & 4-TEST ERROR 1.E-4

[+] NAT=0 and IAT=0 are suggested

Table A2.1 (continued)

25-30	IAT[+]	conditions for stop 0-if NAT test is not satisfied 34-if singular
31-36	IALP	albedo conditions 1-all 2.0 2-diagonal 3-full
37-42	NALP	no. of albedo sets (_0)
43-48	NSS	no. of state variables in a node
49-54	NFEDBK	feedback index 1-no feedback 1-yes
55-60	NJBC[*]	1-node 0-true B.C. 1-node ≠0-estimated B.C. 5-node 0-globally fixed source 5-node ≠0-updated fixed source
Card 3	(I2, 4X, 11I6)	
1-2	NC = 3	card type
3-6	blank	
7-12	IGSYM[++]	global orientation 1-LB 1/4, Lower 1/2 or whole like 2-LT 1/4 or top 1/2 like 3-RB 1/4 4-RT 1/4
13-18	ITEST	test option 1-test input 2-run
19-24	IDSYM[**]	diagonal symmetry (LB--TR) 1-yes 2-no
25-30	LTEST	print option 0-normal 1-node condition 2-file 20 19-Sym. R

[+] NAT=0 and IAT=0 are suggested.

[*] NJBC=0 is suggested. For five node problem always use NJBC=0

[++] IGSYM gives orientation of the assembly in the left bottom section of the core being considered.

[**] Unless all nodes have rotational symmetry, IDSYM=1 can only be used for IGSYM=1 or 4 Remember diagonal symmetry exchange the X--Y

Table A2.1 (continued)

Card 4	(12X, 5E12.6)	
1-12	blank	
13-24	SREF(NSS)	reference state variables
		use as many cards as needed
25-36		
⋮		
61-72		
	must have a card 04 (blank) even if NFEDBK = 1	
Card 5	(6X, 11I6)	
1-6	blank	
7-12	NCOMP(NYY, NXX)	NYY=NY+2 (L--R) NXX=NX+2 (T--B)
		1st and last columns and rows are albedo rows and columns. X-dir. goes first, use as many cards as needed in each dir. initiate a new card for
67-72		different Y
Card 6	(12X, 5E12.6)	
1-12	blank	
13-24	DLX(NX)	X-dir nodal size (L--R)
⋮		use as many cards as needed
61-72		
Card 7	(12X, 5E12.6)	
1-12	blank	
13-24	DLY(NY)	Y-dir nodal size (B--T)
⋮		use as many cards as needed
61-72		

Table A2.1 (continued)

Card 8	(12X, 5E12.6)	
1-12	blank	
13-24	ALP(N2, N2, 2, NALP)	albedo matrices not needed if NALP=0 or if IALP=1 if IALP=2 need only N2 elements in each dir. in each type. first X-dir then Y-dir. use as many cards as needed for each dir. initiate a new card for different dir. N2=NSEG*NG if IALP=3 need a N2*N2 full matrix for each dir. in each type (J,I), I goes first. use as many cards as needed for each J. initiate a new card for different J first X-dir, then Y-dir. $\phi = \alpha J_{\text{NET}}^{\text{in normal direction}}$

Table A2.2 File Definitions Used in Performing the Global/Local Iteration

'RESPONSE' NEEDS

FILE	DESCRIPTIONS	DISK	FILE MODE	RECFM	LRECL	BLKSZZE
6	PRINTOUT	DISK	E	F	132	132
20	OUTPUT INTERFACE FILE	DISK	D	VBS	4096	4096
21	INPUT INTERFACE FILE	DISK	D	VBS	4096	4096
49	State variables, s.p., needed only if NFEDBK>1	DISK	D	VBS	4096	4096
50	Input data	DISK	A	--	--	--
51 to 50+NST	R(0=RJ) s.p., (J,I) J goes first	DISK	D	VBS	4096	4096
50+NST+1 to 50+2*NST	Distributions, s.p. Needed only if NQND$\neq$1 and NSEG=2	DISK	D	--	--	--
50+2*NST+1 to 50+3*NST	R',(IR=R'J),s.p., (J,I) J goes first	DISK	D	VBS	4096	4096
	'QUANDRY' NEEDS					
6	PRINTOUT	DISK	E	F	132	132
10	Input data	DISK	A	--	--	--
20	Input interface file (not needed for initialization)	DISK	D	VBS	4096	4096
21	Output interface file	DISK	D	VBS	4096	4096

Table A2.2 (continued)

FILE	DESCRIPTIONS	DISK	FILE MODE	RECFM	LRECL	BLKSZZE
		'COMPARE' NEEDS				
6	PRINTOUT	DISK	E	F	132	132
7	INPUT data	DISK	A	--	--	--
50	INPUT data	DISK	A	--	--	--
1	Reference data file	DISK	E	VBS	4096	4096
2	Approximate data file	DISK	D	VBS	4096	4096

Appendix 3. Variation of Two-Group Cross Sections With Exposure

The variation of the two-group diffusion coefficients, total cross sections, and fission cross sections with exposure for several compositions in the Vermont Yankee BWR bundle shown in Fig. 2 is illustrated in Figs. A3.1 to A3.3. All cross sections are for a coolant void fraction of 0.4, a fuel temperature of 820 K, and an unrodded state.

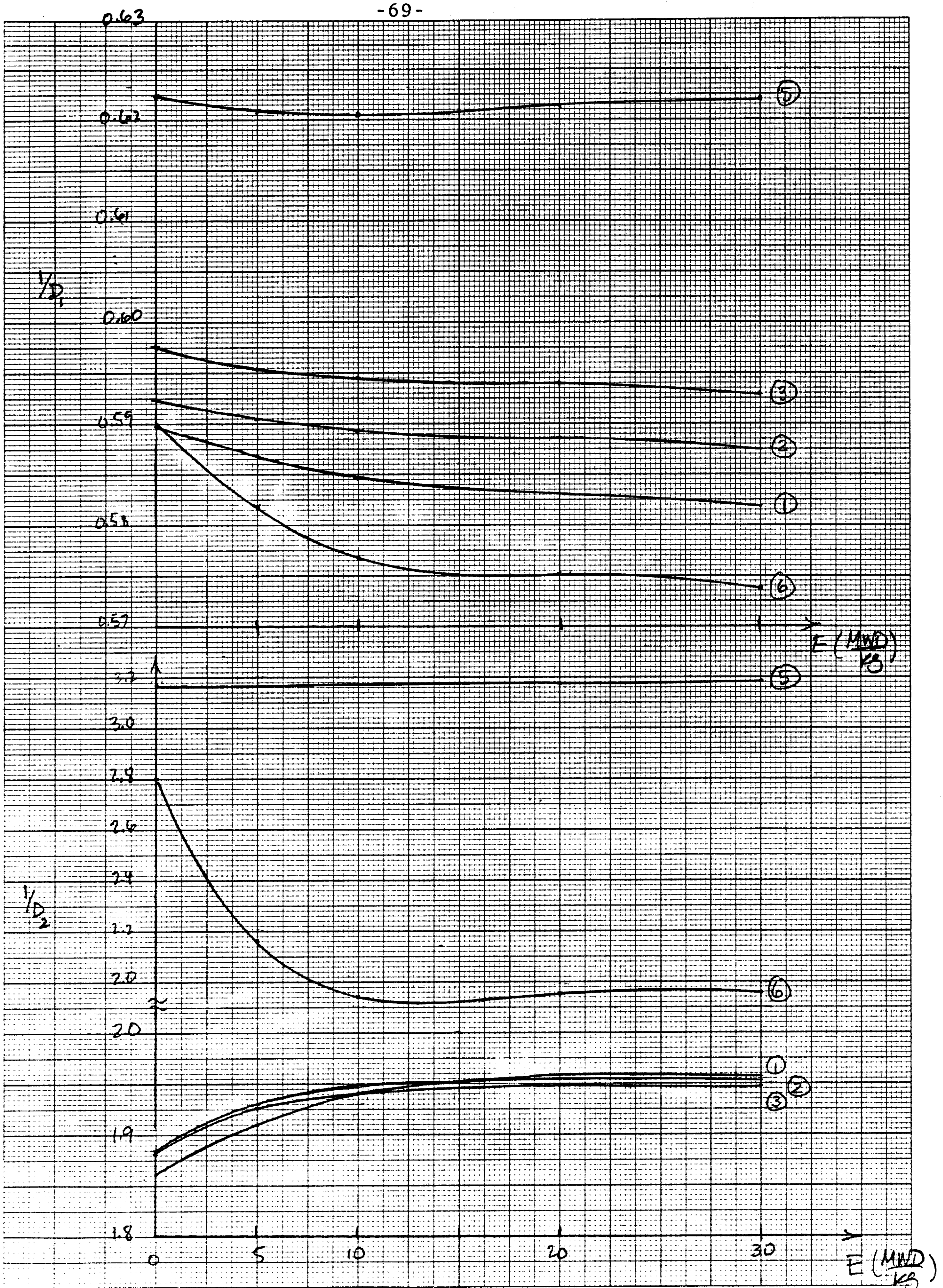

Fig. A3.1 The inverse group diffusion coefficients as functions of exposure for different Compositions in Fig. 2. In all cases, v=0.4 and T=820K.

K-E 10 X 10 TO THE CENTIMETER 18 X 25 CM.
KEUFFEL & ESSER CO. MADE IN U.S.A.
46 1510

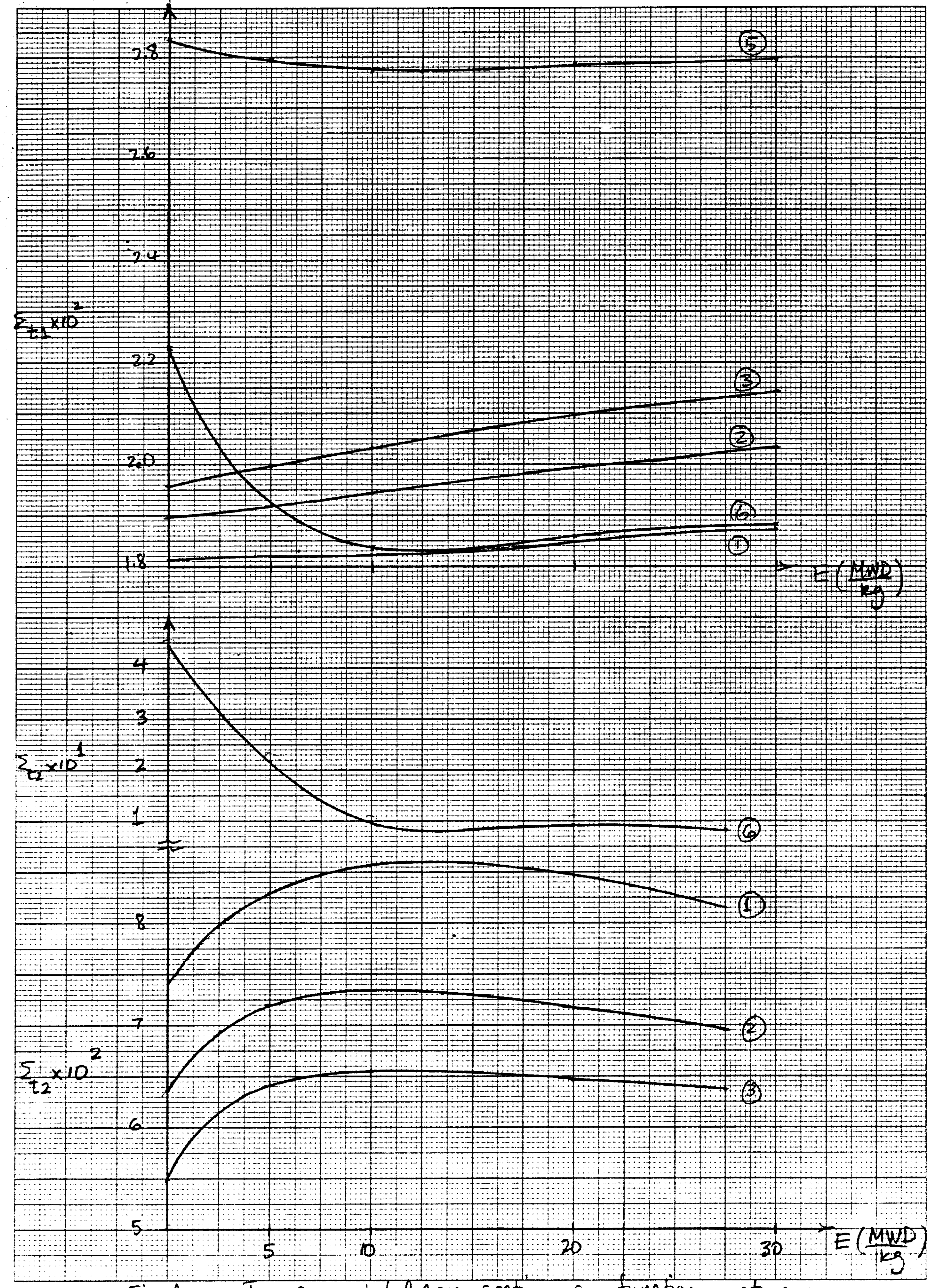

Fig. A3.2 Two-group total cross sections as functions of exposure. The various compositions are defined in Fig. 2.

461510
K+E 10 X 10 TO THE CENTIMETER 18 X 25 CM. KEUFFEL & ESSER CO. MADE IN U.S.A.

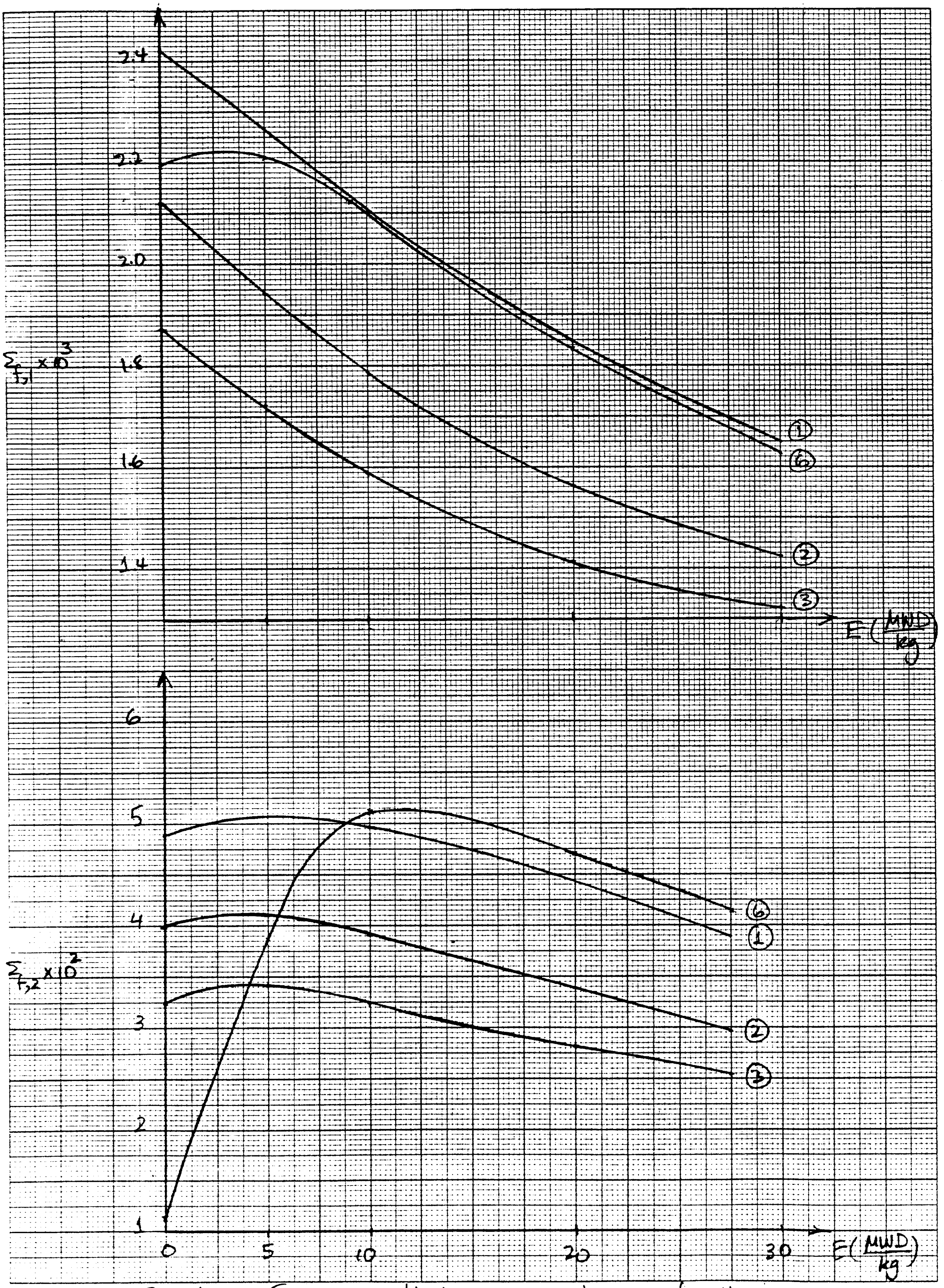

Fig. A3.3 Two-group fission cross sections as functions of exposure.

461510
K+E 10 X 10 TO THE CENTIMETER 18 X 25 CM.
KEUFFEL & ESSER CO. MADE IN U.S.A.